Phenoscaping Reveals Multimodal γδ T Cell Cytotoxicity as a Strategy to Overcome Cancer Cell-Mediated Immunomodulation

Callum Baird Nattress[1,2], Rhianna O'Sullivan[1], Daniel Fowler[2], Colin Hutton[3], Petra Vlckova[1], Jahangir Sufi[1], Magdalena Buschhaus[4], Ewa Basiarz[1], Maria Ramos Zapatero[1], Ferran Cardoso Rodriguez[1], Xiao Qin[1], Ashley Campbell[1], Angeliki Kanouta[2], Vivian S.W. Li[3], Kerry Chester[4], John Anderson[5], Marta Barisa[2], Jonathan P.H. Fisher*[2], and Christopher J. Tape*[1]

[1]Cell Communication Laboratory, Department of Oncology, University College London Cancer Institute, 72 Huntley Street, London, WC1E 6DD, UK.
[2]Innate Immune Engineering Laboratory, Department of Developmental Biology and Cancer, Zayed Centre for Research into Rare Diseases in Children, Great Ormond Street Institute of Child Health, University College London, 20 Guilford Street, London, WC1N 1DZ, UK.
[3]Stem Cell and Cancer Biology Laboratory, The Francis Crick Institute, 1 Midland Road, London, NW1 1AT, UK.
[4]Antibody Medicines Laboratory, Department of Oncology, University College London Cancer Institute, 72 Huntley Street, London, WC1E 6DD, UK.
[5]Department of Developmental Biology and Cancer, Zayed Centre for Research into Rare Diseases in Children, Great Ormond Street Institute of Child Health, University College London, 20 Guilford Street, London, WC1N 1DZ, UK.

Correspondence: *c.tape@ucl.ac.uk, *jonathan.fisher@ucl.ac.uk

Corresponding Authors:
Christopher J. Tape, Cell Communication Laboratory, Department of Oncology, University College London Cancer Institute, 72 Huntley Street, London, WC1E 6DD, UK, c.tape@ucl.ac.uk

Jonathan P.H. Fisher, Innate Immune Engineering Laboratory, Department of Developmental Biology and Cancer, Zayed Centre for Research into Rare Diseases in Children, Great Ormond Street Institute of Child Health, University College London, 20 Guilford Street, London, WC1N 1DZ, UK, jonathan.fisher@ucl.ac.uk

Running Title: γδ **T cell-PDO Phenoscaping**

Conflict of Interest Statement:
J.A. declares founder shares in Autolus Ltd and collaborations with Roche and ALX-Oncology. M.B. is an inventor on patents pertaining to CAR-T cell development and the manufacture of γδ T cells (GB1821321.5, WO2023180759A1, WO2024009075A1). J.F. is an inventor on patents pertaining to engineered γδ T cells and methods for engineering γδ T cells which were used in this research (WO2021148788A1, WO2023180759A1).
K.C. is an inventor on patent WO2021148788A1. DF is an inventor on patent WO2023180759A1.

Abstract

γδ T cells can kill cancer cells via antibody-independent cytotoxicity (AIC) and antibody-dependent cellular cytotoxicity (ADCC). A better understanding of how these cytotoxic mechanisms are impacted by different cancer cells and different T cell donors could help identify improved immunotherapeutic strategies. To test the combinatorial interactions between T cell inter-donor heterogeneity (IDH), cancer cell inter-tumor heterogeneity (ITH), and multimodal γδ T cell killing, we performed a systematic single-cell phenoscaping analysis of >1,000 cultures of γδ T cells and colorectal cancer (CRC) patient-derived organoids (PDO). Phenoscaping analysis of post-translational modification (PTM) signaling, cell-cycle, apoptosis, and T cell immunophenotypes revealed that while unmodified γδ T cells have limited anti-tumor activity, IL-15Rα-IL-15 fusion protein (stIL15)-engineered γδ T cells can kill PDOs via AIC without exogenous cytokine support. However, when stIL15 γδ T cells only killed via AIC, cancer cells reciprocally rewired γδ T cell PTM signal networks in an ITH-specific manner to suppress anti-cancer cytotoxicity. stIL15 γδ T cells could overcome this cancer cell immunomodulation by also engaging B7-H3-targeted ADCC independent of B7-H3 checkpoint activity. Combined AIC and ADCC rescued γδ T cell PTM signaling flux and enabled γδ T cells to kill chemorefactory revival colon cancer stem cells. Together, these results demonstrate that multimodal γδ T cell cytoxicity mechanisms can overcome ITH-specific immunomodulation to kill chemorefractory cancer cells.

Statement of Significance: Single-cell phenoscaping of >1,000 γδ T cell and patient-derived organoid cultures shows that cancer cells suppress anti-cancer γδ T cell cytotoxicity but γδ T cells can use multimodal killing to overcome immunomodulation.

Introduction

Adoptive T cell therapies are an important new class of anti-cancer immunotherapies [1]. Despite the success of αβ chimeric antigen receptor T (CAR-T) cells for the treatment of haematological malignancies, the efficacy of cellular therapies against solid tumours remains limited [2]. Furthermore, the reliance of CAR-T cells on a single killing modality can limit their cytotoxic potential against antigen-heterogeneous cancers [3]. Alternative adoptive cellular therapies based on γδ T cells and NK cells are undergoing evaluation as anti-cancer biotherapeutics, but our understanding of how these cells are regulated by genetic engineering and interactions with heterogenous cancer remains limited.

Vγ9Vδ2 γδ T cells (hereafter γδ T cells) are a subset of cytotoxic T cells that can kill cancer cells via multiple mechanisms [4]. Antibody-independent cytotoxicity (AIC) is achieved by both MHC-independent function of the γδ T cell receptor (TCR) and NK-like receptors such as NKG2D, DNAM-1, and the natural cytotoxicity receptors (NCRs) NKp30, NKp44, and NKp46 [5]. Additionally, γδ T cells can perform antibody-dependent cellular cytotoxicity (ADCC) via Fcγ receptor CD16 (FcγRIII) and tumour-bound IgG [6, 7, 8]. γδ T cells can be genetically engineered [9, 8], are safe in the allogeneic setting [10], and can be readily expanded for clinical use [4]. The various γδ T cell killing modalities, as well as their ability to persist within and serially kill solid tumours, can be further enhanced via engineered secretion of common γ-chain cytokines [9, 8].

Colorectal cancer (CRC) is a solid tumour of the colonic and rectal epithelium that results in the death of >900,000 people per year [11]. CRC tumours are complex heterocellular systems that possess substantial non-genetic plasticity [12] and an immunosuppressive tumour microenvironment (TME) [13]. Although ~15% of patients display microsatellite instability (MSI) leading to high tumour mutational burden (TMB) and remarkable neoadjuvant immune-checkpoint blockade (ICB) responses [14], the majority of CRC patients have microsatellite stable (MSS) disease with a low TMB and respond poorly to immunotherapies [15]. Furthermore, CRC cells possess high phenotypic plasticity [16, 17] that can drive non-genetic resistance to standard-of-care chemotherapies via stem cell transdetermination from chemosensitive proliferative colonic stem cells (proCSC) to chemorefractory revival colonic stem cells (revCSC) [12, 18]. Consequently, there is a desperate need to develop new treatment options for chemoresistant revCSC-dominant MSS CRC.

A primary challenge in the treatment of cancer is the large variance in phenotype and treatment response between patients — commonly known as 'inter-tumour heterogeneity' (ITH) [19]. In the context of allogeneic cellular therapies, the complexity of ITH is further compounded by variability between cell products derived from different PBMC donors — so-called 'inter-donor heterogeneity' (IDH) [20, 21]. How cancer ITH interacts with γδ T cell IDH across a range of T-cell killing mechanisms is unknown.

Phenoscaping is an emerging experimental technique that combines systematic high-throughput perturbations with high-dimensional single-cell analysis to map the phenotypic regulators of a dynamic cellular system [22]. We recently used phenoscaping to map the cell-intrinsic and -extrinsic regulators of colonic stem cell plasticity [23], but to date, no phenoscaping study of T-cell – cancer cell interactions has been reported.

Here, we present a large-scale single-cell phenoscaping analysis of γδ T cell interactions with Patient-Derived Organoid (PDO) models of CRC to chart the regulators of multimodal γδ T cell cytotoxicity across cancer ITH and T-cell IDH. Using Thiol-reactive Organoid Barcoding *in situ* mass cytometry (TOB*is* MC) [24, 25] we studied post-translational modification (PTM) signalling, cell-state, apoptosis, and immunophenotype of γδ T–PDO interactions in 3D across >1,000 perturbations at single-cell resolution.

Phenoscaping analysis revealed that unmodified γδ T cells have variable expansion phenotypes and poor cytotoxicity against CRC PDOs. However, γδ T cells engineered to express an IL-15Rα-IL-15 fusion protein (stIL15) [26, 8] are cytotoxic against CRC PDOs, but can be reciprocally immunomodulated by PDOs in an ITH-specific manner, including global rewiring of γδ T cell PTM signalling networks. We find that tumour-derived γδ T cell immunomodulation can limit anti-cancer killing when γδ T cells use AIC alone, but that immunomodulation can be overcome by cancer cell opsonisation using anti-B7-H3 monoclonal antibody (mAb) therapy, which engages γδ T cell ADCC capacity. Crucially, we find that engineered γδ T cells can kill MSS PDOs that are enriched for chemorefractory revCSCs. Taken together, these results demonstrate the value of high-throughput cellular therapy phenoscaping and reveal that γδ T cell multimodal cytotoxicity can overcome immunomodulation to kill chemoresistant cancer cells.

Materials and Methods

Organoid Culture

CRC PDOs were obtained from the Human Cancer Models Initiative with written informed consent (Sanger Institute, Cambridge, UK) [27] and expanded in 3x 25 µL droplets of Growth Factor Reduced Matrigel (Corning 354230) per well of a 12-well plate (Helena Biosciences 92412T). Each well was supplemented with 1 mL of PDO expansion media comprising Advanced DMEM F/12 (Thermo 12634010) containing 2 mM L-glutamine (Thermo 25030081), 1 mM N-acetyl-L-cysteine (Sigma A9165), 10 mM HEPES (Sigma H3375), 500 nM A83-01 (Generon 04–0014), 10 mM SB202190 (Avantor CAYM10010399-10), and 1X B-27 Supplement (Thermo 17504044), 1X N-2 Supplement (Thermo 17502048), 50 ng mL^{-1} EGF (Thermo PMG8041), 10 nM Gastrin I (Sigma SCP0152), 10 mM Nicotinamide (Sigma N0636), and 1X HyClone Penicillin-Streptomycin Solution (Fisher SV30010), and conditioned media produced as described in [28] at 5% CO_2, 37°C. L-cells for conditioned media production were obtained from Shintaro Sato (Research Institute of Microbial Diseases, Osaka University, Osaka, Japan) [29]. PDOs were dissociated into single cells with 1X TrypLE Express Enzyme (Gibco 12604013) (incubated at 37°C for 20 min) and passaged every 5-10 days. For the first 24 hours after dissociation, media was also supplemented with 10 µM Rho-associated protein kinase inhibitor (ROCKi) (Y-27632, Sigma Y0503). L-cells for conditioned media production were obtained from Shintaro Sato (Research Institute of Microbial Diseases, Osaka University, Osaka, Japan). To aid cell-type-specific visualization and gating, CRC PDOs were transfected with H2B-RFP (Addgene 26001).

Generation of CRISPR B7-H3^{KO} PDOs

A custom lentivirus containing a GFP reporter, Cas9 and gRNA against B7-H3 (CTGGTGCACAGCTTTGCTG) was ordered from Merck. PDOs were dissociated into single cells with 1X TrypLE Express Enzyme (Gibco 12604013) (incubated at 37°C for 20 min). Single-cell PDOs were transduced at an MOI of 5 in PDO expansion media supplemented with 10 µM ROCKi and 8 µg/mL Polybrene (Merck TR-1003-G) with spinoculation at 300 x *g* for 1 hour at room temperature. Following transduction, single-cell PDOs were passaged and expanded as normal. Upon reaching a sufficient number for cell-sorting, PDOs were dissociated into single-cells and washed in FACS buffer (PBS (Gibco) supplemented with 1 mM (Sigma 03690), 25 mM HEPES and 1% FBS). Cells were stained with 1 µg/mL of anti-human B7-H3 primary antibody (Prof. Kerry Chester, UCL Cancer Institute, London, UK) and 1 µg/mL of goat anti-human IgG secondary antibody (Thermo A-21445). Cells negative for B7-H3 were bulk sorted through a BD FACSAria™ III into collection media (50% PDO expansion media and 50% FBS supplemented with 10 µM ROCKi) and grown as normal. PDOs underwent a repeat bulk sort following multiple passages to select a stable B7-H3^{KO} population. 100% B7-H3^{KO} efficiency of the twice-sorted PDO population was confirmed with B7-H3 gene amplification and Sanger sequencing.

PBMC Isolation

This study was approved by a national ethics committee (West Midlands HRA, 14/WM/1253) and complied with the WMA declaration of Helsinki with written informed consent. Leukopaks from healthy donors were purchased from Cambridge Bioscience (Cambridge, UK) and PBMCs were isolated by density-adjusted centrifugation using Lymphopure™ density gradient medium (BioLegend 426201). Residual red blood cells were removed using ammonium-chloride-pottasium (ACK) lysing buffer (Thermo A1049201) and platelets were removed with slow-speed centrifugation. PBMCs were immediately frozen in a freezing solution containing 10% DMSO, with storage complying with the Human Tissue Act 2004. Owing to the size and longitudinal nature of the screen, cryopreserved PBMCs were used so that a consistent bank of γδ T cell donors could be utilised across multiple batches of experiments.

γδ T cell Expansion

Cryopreserved PBMCs were thawed and rested overnight in RPMI 1640 medium supplemented with 1X GlutaMAX™ and 10% (v/v) FBS (Gibco 10082147) at 5% CO_2, 37°C. For Vγ9Vδ2 expansion, overnight rested PBMCs were plated in tissue-culture treated plates at 2 x 10^6 cells/cm^2 in fresh media and stimulated with 5 µM zoledronic acid (ZOL) (Actavis) and IL-2 (100 IU/mL; Aldesleukin, Novartis). Unless otherwise stated, IL-2 was replenished every 2-3 days by removing 50% of the media from the well and replacing with fresh media containing IL-2 (200 IU/mL). γδs were expanded until D12 at which point they were harvested for experimental use and flow cytometry immunophenotyping. By D12, γδ T cells typically represent the predominant cell type, with remaining populations of NK cells and $\alpha\beta$ T cells varying by donor.

Lentiviral Vectors

Gene constructs containing both enhanced green fluorescent protein (eGFP) and stabilised IL-15 (stIL15) were designed using SnapGene 2.8.3. Gene blocks were synthesised by Twist Bioscience (California, USA) and cloned into a pCCL.SFFV RdPro-pseudotyped lentiviral vector using standard restriction enzyme cloning. eGFP-stIL15 lentivirus was produced in-house and was titred on HEK293T cells (CVCL_0063) with the number of titratable units/mL determined by flow cytometry.

Lentiviral Transduction of γδ T cells

Following 48 hours of ZOL and IL-2 stimulation, lentivirus was diluted in Opti-MEM™ (Thermo 31985062) and added directly to the γδ culture wells at an MOI of 4. Spinoculation and transduction enhancers were not used for lentiviral transduction. Transduced γδs were expanded until D12 at which point they were harvested for experimental use and flow cytometry immunophenotyping. Transduction efficiency was calculated as the percentage of live Vδ2 expressing GFP.

Flow Cytometry

Flow cytometric analysis was performed using a FACSymphony™ A5 flow cytometer (BD Biosciences, SCR_022538). Data were acquired using BD FACSDiva (Version 8.0.1) and analysed using FlowJo 10.10.0 and Cytobank (Beckman Coulter). Compensation was calculated with the use of OneComp eBeads (Thermo 01-1111-41) stained with single-colour antibodies. CRC PDO B7-H3 antigen density was estimated using the BD Quantibrite PE kit (BD Biosciences 340495) as per the manufacturer's protocol and a primary anti-human B7-H3 PE antibody (Miltenyi 130-120-712).

Anti-B7-H3 Monoclonal Antibody

The anti-B7-H3 monoclonal antibody was obtained from a murine single chain Fv (scFv) phage-display library constructed as previously described [30]. B7-H3 binding scFvs were identified by panning and phage monoclonal ELISA. The scFv was subcloned into a chimeric hIgG1 format using a G1m1,17 heavy chain allotype and produced as a full antibody by Evitria AG (www.evitria.com) using transient expression in CHO cells and protein A purification. Fc null versions of the same B7-H3 mAb clones were generated via the incorporation of 'LALA' mutations into the Fc domain (L234A/L235A), and were also produced by Evitria.

Co-Culture of CRC PDOs with γδ T cells

PDO-γδ T cell co-cultures were always performed with D12-expanded γδ T cells. On D7 of γδ T cell expansion, PDOs were dissociated into single cells with 1X TrypLE Express Enzyme (Gibco 12604013) (incubated at 37°C for 20 min) and expanded in 3x 25 µL droplets of Growth Factor Reduced Matrigel (Corning 354230) per well of a 12-well plate (Helena Biosciences 92412T). Each well was supplemented with 1 mL of Advanced DMEM F/12 (Thermo 12634010) containing 2 mM L-glutamine (Thermo 25030081), 1 mM N-acetyl-L-cysteine (Sigma A9165), 10 mM HEPES (Sigma H3375), 1X B-27 Supplement (Thermo 17504044), 1X N-2 Supplement (Thermo 17502048), 50 ng mL^{-1} EGF (Thermo PMG8041), 10 nM Gastrin I (Sigma SCP0152), 10 mM Nicotinamide (Sigma N0636), 500 nM A83-01 (Generon 04–0014), 10 mM SB202190 (Avantor CAYM10010399-10) and 1X HyClone Penicillin-Streptomycin Solution (Fisher SV30010) at 5% CO_2, 37°C for 4 days. For the first 24 hours after dissociation, media was also supplemented with 10 µM ROCKi (Y-27632, Sigma Y0503). On D11 of γδ T cell expansion (D5 of PDO expansion), PDOs were starved in reduced media, consisting of Advanced DMEM F/12 containing only 2 mM L-glutamine, 1 mM N-acetyl-Lcysteine, 10 mM HEPES, 1X B-27 Supplement, 1X N-2 Supplement, 10mM Nicotinamide, and 1X HyClone-Penicillin Streptomycin Solution, at 5% CO_2, 37°C for 24 hours before experimental seeding. On the day of experimental seeding, D5-expanded PDOs and D12-expanded γδ T cells were seeded as mono- and co-cultures in flat-bottom 96-well plates (Helena Biosciences 92696T) in 50 µL Matrigel stacks with 300 µL of reduced media for 48 hours. PDOs and γδ T cells were seeded at a density of ~1.5 x 10^3 and 3.75 x 10^5 cells/well, respectively. PDOs are complex, heterocellular 3D structures that comprise tens to hundreds of individual cancer cells per PDO, although significant heterogeneity in size and cellular density exist between patients. Single-cell counts from dissociated PDOs suggest an E:T ratio of ~5:1 to 1:1 in this manuscript, based on a density of 1.5 x 10^3 PDOs/well. When specified, cultures were treated with 1 µg/mL of anti-human B7-H3 IgG (Prof. Kerry Chester, UCL Cancer Institute, London, UK). After 24 hours of culture, all wells received a 50% media change with fresh reduced media. Experiments were ended after 48 hours of co-culture and processed for thiol-reactive organoid barcoding *in situ* (TOB*is*) mass cytometry (see below).

Thiol-reactive Organoid Barcoding *in situ* (TOB*is*) Mass Cytometry

PDO monocultures, γδ T cell monocultures and PDO-γδ T cell co-cultures were analysed using the TOB*is* mass cytometry protocol described in Sufi & Qin *et al* [25]. In brief, after 48 hours, PDO-γδ T cell cultures were incubated with 25 mM (5-Iodo-20-deoxyuridine) (^{127}IdU) (Standard BioTools 201127) at 37°C for 30 min, and 5 min before the end of this incubation, 1X Protease Inhibitor Cocktail (Sigma, P8340) and 1X PhosSTOP (Sigma 4906845001) were added into the media. Each well was then fixed in 4% PFA/PBS (Thermo J19943K2) for 1 h at 37°C. PDO-γδ T cells were washed with PBS, dead cells were stained using 0.25 mM ^{194}Cisplatin (Standard BioTools 201194), and PDO-γδ Tcells were barcoded *in situ* with 126-plex (9-*choose*-4) TOB*is* overnight at 4°C. Unbound barcodes were quenched in 2 mM GSH and all PDO-γδ T cells were pooled. PDO-γδ T cells were dissociated into single cells using 0.875 mg mL^{-1} Dispase II (Thermo 17105041), 0.2 mg mL^{-1} Collagenase IV (Thermo 17104019), and 0.2 mg mL^{-1} DNase I (Sigma DN25) in C-Tubes (Miltenyi 130-096-334) via gentleMACS Octo Dissociator with Heaters (Miltenyi 130-096-427, SCR_020271). Single PDO and γδ T cells were washed in cell staining buffer (CSB) (Standard BioTools 201068) and stained with extracellular rare-earth metal conjugated antibodies for 30 min at room temperature. PDO-γδ T cells were then permeabilised in 0.1% (v/v) Triton X-100/PBS (Sigma T8787), 50% methanol/PBS (Fisher 10675112), and stained with intracellular rare-earth metal conjugated antibodies for 30 min at room temperature. PDO-γδ T cells were then washed in CSB and antibodies were cross-linked to cells using 1.6% (v/v) FA/PBS for 10 min. PDO-γδ T cells were incubated in 125 nM^{191} Ir/^{193} Ir DNA intercalator (Standard BioTools 201192A) overnight at 4°C. PDO-γδ T cells were washed, resuspended in cell acquisition solution plus (CAS+) (Standard BioTools 201244) with 2 mM EDTA (Sigma 03690), and analysed using a CyTOF XT (Standard BioTools, SCR_02634) at 200–400 events s^{-1}.

Chemotherapy Treatment of CRC PDOs

We recently performed a phenoscape of >2,500 drug-treated CRC PDO and CAF cultures [18]. We leveraged the cytotoxicity data from PDO monocultures treated with a range of physiologically relevant concentrations of SN-38 (1 nM - 100 nM), 5-FU (0.2 µM - 200 µM) and oxaliplatin (2 nM - 200 nM) as a benchmark of chemosensitivity. The maximum apoptosis response achieved for each chemotherapy was chosen as a comparison for γδ T cell cytotoxicity.

Mass Cytometry Data Processing

Multiplexed FCS files were debarcoded into individual experimental conditions using the Zunder Lab Single Cell Debarcoder tool (https://github.com/zunderlab/single-cell-debarcoder) [31]. Debarcoded FCS files were uploaded to Cytobank and gated for Gaussian parameters and DNA content (^{191}Ir/^{193}). Epithelial PDO cells were gated as Pan-CK$^+$EpCAM$^+$; γδs were gated as CD45$^+$CD3$^+$γδ-TCR$^+$. Exported PDO and γδ cells were arcsinh transformed and mean-centred across acquisition batches before downstream analysis. The therapeutic apoptosis achieved by γδ T cells was calculated relative to the baseline apoptosis measured in PDO monoculture controls.

In Vivo Studies: Circulating γδ T cell Analysis

Immune-deficient female 6-week-old NOD.Cg-*Prkdc*^{scid} *Il2rg*^{tm1Wjl}/SzJ (NSG) mice were obtained from the Francis Crick Institute Biomedical Research Facility and housed in individually-ventilated cages with a maximum of 5 mice per cage. Mice were used at ~9 weeks of age for experiments. All experiments were performed with ethical approval (Animal Welfare Ethical Review Body) under Home Office Project License PPL PP4021677. Mice were treated with an intravenous (i.v.) injection into the tail vein of PBS or 10 x 10^6 unmodified or stIL15-γδ T cells. After 7 days, mice were prepared for terminal cardiac puncture under general anaesthesia. 2 hours before cardiac puncture, mice received an intraperitoneal (i.p.) injection of 200 µg ^{127}IdU to label cells undergoing S-phase. Following cardiac puncture, red blood cells were removed with ACK lysing buffer (Thermo A1049201) and PBMCs were washed in PBS before fixation with 4% PFA/PBS (Thermo J19943K2) at room temperature for 10 minutes. Fixed PBMCs from each mouse were barcoded with unique TOB*is* barcodes for 2 hours at room temperature. Unbound barcodes were quenched in 2 mM GSH before all PBMCs were pooled into a single tube. Cells were then stained for mass cytometry as described above.

Earth Mover's Distance (EMD) and $\bar{x}$EMD

Earth Mover's Distance (EMD) scores were calculated using the Python package scprep. Standard EMD scores were calculated between probability distributions (markers) across experimental conditions using defined controls as references. Signs were applied to EMD scores to denote an increase or decrease in expression. $\bar{x}$EMD represents a coordinate sliced Wasserstein distance [32] and describes the absolute average difference across all measured markers between experimental conditions irrespective of direction. $\bar{x}$EMD was calculated by taking the absolute EMD values (no sign applied) for all markers and averaging them. $\bar{x}$EMD scores were calculated between stIL15-γδ T cell

monoculture controls and those in co-culture with CRC PDOs; this allowed the quantification of the average change in stIL15-γδ T cell immunophenotype, PTM-signalling and cell-state due to immunomodulation by PDOs.

DREMI and ΔDREMI

k -Nearest Neighbours Density-Resampled Estimate of Mutual Information (*k* NN-DREMI) [33] scores were computed with the Python package *scprep* [34]. *k* NN-DREMI scores among 11 PTMs were calculated, which yielded a total of 110 PTM-PTM combinations for each stIL15-γδ T cell condition. To quantify the rewiring of stIL15-γδ T cell PTM signalling networks, the differences in PTM-PTM combinations across conditions were calculated (Δ*k* NN-DREMI (referred to as ΔDREMI)). These pairwise calculations were computed for all conditions, either comparing stIL15-γδ T cell monocultures to untreated co-cultures, or untreated co-cultures compared to co-cultures with B7-H3 mAb. ΔDREMI scores for each condition were visualised via PHATE.

PHATE

Potential of heat diffusion for affinity-based transition embedding (PHATE) is a non-linear dimensionality reduction method that aims to preserve the local and global structure of datasets [35]. A variety of data matrices can drive PHATE embeddings, including EMD scores and ΔDREMI scores, whereby the resulting embedding captures maximal variance across all the dataset dimensions. Conclusions can be made surrounding the relative distance of points within a PHATE embedding, which are linked to underlying similarities or differences in the chosen markers of a mass cytometry panel (as captured by EMD calculation).

scRNA-seq of CRC PDOs

scRNA-seq of CRC PDOs was performed using the SPLiT-seq method described in Ramos Zapatero *et al*. [18]. In brief, PDOs were cultured in triplicate as described above for 72 hours with fresh reduced media replaced every 24 hours. PDOs were harvested and dissociated into single cells using TrypLE (Thermo 12604013) incubated for 10 minutes at 37°C on a heated orbital shaker at 300 rpm. Cells were filtered through a 35 µM filter and re-suspended in 1 mL of PBS supplemented with 1.25 µL Protectorase RNase inhibitor (Merck 3335402001) and 2.5 µL Superase RNase inhibitor (Thermo AM2694). Cells were fixed, permeabilised, counted and 5% (v/v) DMSO was added before aliquoting and freezing in a Mr Frosty at -80°C. One complete SPLiT-seq experiment was performed per two PDOs studied (five independent SPLiT-seq runs total). Split-pool barcoding combinatorial indexing was performed as per the SPLiT-seq protocol[36] with minor modifications. Briefly, cells were thawed and reverse transcribed in the barcode-RT1 plate, followed by two rounds of pooling and ligation in the ligation-L2 and ligation-L3 plates. Cells were then counted and aliquoted into sub-libraries of approximately 12,500 cells, lysed and frozen at -80°C until library preparation.

Following split-pool barcoding, 4 sub-libraries were carried forward for cDNA isolation, amplification and library generation as described in Ramos Zapatero *et al.* [18]. Libraries were then pooled together equally, loaded onto an Illumina Novaseq (200 cycle NovaSeq 6000 S2 Reagent Kit v1.5) and sequenced within the following format: R1:74-i7:06-i5:00-R2:86 to yield a paired-end read structure comprising cDNA transcriptomic information in read 1 and barcoding information in read 2. The data were demultiplexed using the sublibrary i7 indexes and reads aligned to the GRCh38 reference genome using the zUMIs package (v2.9.7) [37] with STAR (v2.7.3a), filtering on a whitelist of permitted cell barcodes and merging cells that shared PolyA and Random Hexamer RT1 barcodes from the same RT well plate position with identical L2 and L3 barcodes, including reads originating from exons and introns. Cell barcodes were collapsed based on a 2 hamming distance of close cell barcodes and UMIs on a 1 hamming distance of UMI sequence. A cell x gene digital gene expression matrix (DGE) was generated for each library.

scRNA-seq Data Preprocessing and Analysis

For all sequencing runs, the DGE of each sublibrary was processed using the splitRtools package (https://github.com/TAPE-Lab/splitRtools) to annotate cell barcode well locations and sample identities, and perform initial QC. Downstream analysis was performed in Scanpy [38]. Sublibrary DGEs were merged and low-quality cells were excluded using the following parameters; >32,500 unique molecular identifiers (UMIs) and <1000 UMIs, >7000 genes and <300 genes, >20% mitochondrial transcripts, >0.4 UMI/read ratio and genes detected in fewer than 25 cells. Neotypic doublets were identified and removed using Scrublet [39] with an expected doublet rate of 3%. Cells were then normalised using count-based normalisation with a scaling factor of 10,000 excluding highly expressed genes comprising >5% of total counts per cell. The normalised data were then natural log transformed for downstream analysis. Data were scaled and PCA performed over 5000 variable genes, a neighbourhood graph was constructed based on the first 50 PCs as input and Leiden clustering was performed to generate clusters. Once all scRNA-seq datasets had been filtered as above, the final DGEs were merged, ultimately yielding a dataset of 89,894 high-quality single cells.

Using the merged dataset PDO specific proCSC and revCSC signatures were computed by scoring each PDO epithelial cell for literature-derived proCSC and revCSC signatures identified by Opzoomer *et al.* (bioRxiv 2024.02.23.581433) with the score_genes function in Scanpy using default settings on Log-Normalised data. Scores were computed using a defined set of genes and comparing their average relative expression against a reference set of genes, as previously described in Satija *et al.* [40]. Following gene scoring per cell, the stem cell index was calculated by subtracting the proCSC score from the revCSC score to determine the relative distribution of different stem cell signatures within each PDO, as described in Vazquez *et al.* [41].

Statistical Analyses

All statistical analyses were performed using GraphPad Prism 10.1.1. P values of less than 0.05 were considered statistically significant.

Data Availability Statement

Raw and processed CyTOF data and illustrations are available as a Community Cytobank project 1551 (https://community.cytobank.org/cytobank/projects/1551). The raw scRNA-seq data generated in this study are publicly available at BioProject PRJNA1308308 (https://www.ncbi.nlm.nih.gov/bioproject/1308308). Processed scRNA-seq data generated in this study are publicly available at Zenodo project 15827759 (https://zenodo.org/records/15827759). All other raw data generated in this study are available upon request from the corresponding author.

Code Availability

Code to reproduce figures in this paper can be found at: https://github.com/callumnattress/Nattress-et-al-Phenoscaping.

Results

stIL15 Engineering Supports γδ T Cells in 3D ECM

Solid cancer TMEs are often nutrient-starved and immunosuppressive [42]. In CRC, the altered metabolic environment can disrupt communication between resident TME leukocytes and contribute towards immunosuppression [43]. Therefore, to survive and function within the TME anti-cancer cellular therapies must retain viability in a 3D extracellular matrix (ECM) under low-serum conditions. Previous work has demonstrated that γδ T cells engineered to overexpress an IL-15Rα-IL-15 fusion protein (stIL15) have increased expansion and cytotoxicity compared to unmodified γδ T cells in simple 2D culture systems [8]. To investigate whether constitutive stIL15 secretion could support γδ T cells in a 3D ECM culture without exogenous growth factor or cytokine support, we expanded γδ T cells from frozen PBMCs of x7 healthy donors (A-G) (Table S1) (Table S2) in either an unmodified state or following lentiviral transduction to secrete stIL15 (Figure S1a-d) [26, 8, 44]. We then analysed γδ T cell phenotypes immediately after expansion (Table S3).and following 48 hours of culture in 3D Matrigel without IL-2 or serum support (Figure 1a).

Immediately following expansion, unmodified γδ T cells were >60% viable, increasing to >90% when transduced with stIL15 (Figure 1b). stIL15 also increased γδ T cell purity and expansion but did not alter CD16 expression. Lentiviral transduction efficiencies of >50% were routinely achieved (Figure S1e). These results demonstrate that both unmodified γδ T cells and stIL15-γδ T cells are viable from a range of healthy donors immediately following expansion.

By contrast, we found that unmodified γδ T cells and stIL15-γδ T cells had dramatically divergent phenotypes following serum and cytokine-depleted 3D culture (Figure 1c). We have previously demonstrated that thiol-reactive organoid barcoding *in situ* mass cytometry (TOB*is* MC) enables high-throughput analysis of post-translational modification (PTM) signalling, cell-state, and apoptosis of 3D heterocellular cultures [24, 25]. Here we applied TOB*is* MC to study the immunophenotype of γδ T cells in 3D ECM (Table S4). TOB*is* MC analysis revealed that unmodified γδ T cells were 40-70% apoptotic (cPARP $[D214]^+$) after 48 hours in 3D culture without IL-2 or serum (Figure 1d). By comparison, stIL15-γδ T cells were 90-95% viable in 3D, and retained between 10-45% S-phase entry (IdU^+) following 48-hour culture, compared to <5% in unmodified γδ T cells (Figure 1e). γδ T cell S-phase correlated with transduction efficiency, highlighting the donor-specific nature of γδ T cell phenotypes (Figure S1f).

Earth Mover's Distance (EMD) is an optimal transport metric that can quantify shifts between probability distributions of markers across different experimental conditions [45, 46]. EMD analysis of unmodified and stIL15-γδ T cells across all donors revealed that stIL15 activated pSTAT3 $[Y705]^+$, pSTAT5 $[Y694]^+$, pZAP70 $[Y319/Y352]^+$, and pSLP76 $[Y128]^+$ across all donors. Furthermore, stIL15 up-regulated several T cell activation markers including granzyme B, perforin, and CD69 across all donors (Figure 1f). Although engineering did not affect post-expansion %CD16 expression (Figure 1b), stIL15-γδ T cells maintained higher CD16 expression relative to unmodified controls following serum and cytokine starvation in 3D culture (Figure 1f). Changes in γδ T cell immunophenotype and PTM signalling were not induced by viral exposure during transduction and were dependent on stIL15 expression (Figure S1g-i).

Similar results were observed *in vivo*. Whilst unmodified γδ T cells rapidly perished to undetectable levels, stIL15-γδ T cells continued to persist and even proliferate in the circulation one-week following intravenous infusion into tumour-free NOD.Cg-*Prkdc*^{scid} *Il2rg*^{tm1Wjl}/SzJ (NSG) mice (Figure S2a-d). Moreover, evaluation of transduced (GFP^+) *versus* non-transduced (NT) (GFP^-) γδ T cells from stIL15-γδ T cell infused mice showed that transduced γδ T cells support and maintain the NT γδ T cell component of the product *in vivo* (Figure S2e-g). In addition to enhanced survival of NT γδ T cell bystanders, stIL15 expression increased GFP^+ cell NKp30, CD16, CD69 and checkpoint receptor expression (Figure S2h). Collectively, these results demonstrate that stIL15 improves the expansion, viability, and cytotoxic potential of γδ T cells across a range of healthy donors in 3D culture.

Phenoscaping Analysis of γδ T Cell CRC PDO Cytotoxicity

Phenoscaping is an emerging experimental approach that integrates systematic high-throughput perturbations with high-dimensional single-cell analysis to identify phenotypic regulators within dynamic cellular systems [22]. Recently, we applied phenoscaping to uncover the cell-intrinsic and -extrinsic regulators of colonic stem cell plasticity [23]. However, to date, phenoscaping has not been applied to map interactions between T-cells and cancer cells.

To systematically explore γδ T cell cytotoxicity, we performed a phenoscaping analysis of γδ T cells from x7 healthy donors (A-G), +/- stIL15, +/- co-culture with an MSI^+ CRC patient-derived organoid 27 (PDO27). To investigate the contribution of ADCC, γδ T cells and PDO27 were also cultured +/- 1 μg/mL anti-B7-H3 monoclonal antibody (mAb) (Figure 2a). B7-H3 is a tumour-associated antigen that is over-expressed in multiple solid cancers [47], including CRC [48], and is being targeted as a tumour-associated antigen in several clinical trials [49]. This systematic phenoscaping approach allowed us to study γδ T cell inter-donor heterogeneity (IDH), stIL15 engineering, AIC, and ADCC killing in a single experiment.

Single-cell analysis of x180 PDO-γδ T cell 3D cultures revealed that γδ T cell phenotype is influenced by a range of factors, including PBMC donor, stIL15 transduction, and interactions with PDOs (Figure 2b). We found that γδ T cells induced PDO apoptosis in a donor-specific manner (Figure 2c) and stIL15 significantly increased AIC and total anti-PDO cytotoxicity in the presence of B7-H3 mAb in 6/7 donors (Figure 2d). The therapeutic apoptosis achieved by γδ T cells was calculated relative to the baseline apoptosis measured in PDO monoculture controls. We found that against this MSI^+ PDO, the majority of stIL15-γδ T killing was performed via AIC, although ADCC could further increase PDO killing in 6/7 donors (Figure 2d) independent of %CD16 expression in both unmodified and stIL15-γδ T cells (Figure S3a). This suggests that γδ T cells kill CRC cells via multiple cytotoxic mechanisms (Figure S3b-c). Interestingly, stIL15-γδ T cells used a greater proportion of AIC to achieve maximal therapeutic apoptosis relative to unmodified γδ T cells (Figure S3b). CRISPR knockout of PDO B7-H3 inhibited ADCC, demonstrating stIL15-γδ T cell ADCC is antigen-specific (Figure 2e). Moreover, AIC against B7-H3-KO CRC was identical to B7-$H3^+$ CRC, suggesting that – in the context of this assay – B7-H3 does not exert cytotoxicity-suppressing checkpoint effects over γδ T cells.

Unlike small molecules or biologics, cellular therapies are dynamic biological systems that can be regulated by their environment. To quantify how PDOs reciprocally alter γδ T cells, we calculated the absolute mean EMD ($\bar{x}$EMD) for each stIL15-γδ donor when interacting with cancer cells. $\bar{x}$EMD represents a coordinate sliced Wasserstein distance [32] and provides the mean difference between two cell populations for the absolute value of all markers measured — in this case, immunophenotype, PTMs and cell-state, irrespective of direction. Compared to stIL15-γδ T cell monocultures, $\bar{x}$EMD found that PDOs consistently alter the immunophenotype, PTM expression, and cell-state of unmodified and stIL15-γδ T cells across all donors (Figure 2f, Figure S3d). In unmodified γδ T cells, co-culture was predominantly associated with decreased apoptosis and a general increase in PTM signalling (Figure S3e, Figure S4a-b), although, decreases in granzyme B and perforin occurred (Figure S4b) which may be due to the poor cytotoxicity by unmodified γδ T cells or immunomodulation (Figure 2d). Notably, PDOs decreased both apoptosis and S-phase in stIL15-γδ T cells, implying a slowing of cell-cycle progression (Figure 2g) (Figure S3e) (Figure S4a). EMD analysis of stIL15-γδ T cells relative to monoculture controls revealed that stIL15-γδ T cell PTM signalling and immunophenotype are altered by PDOs (Figure 2h). Most donors experienced increased pZAP70 and pSLP76 signalling during both AIC +/- mAb, alongside decreased pNF-κB and pERK signalling as well as decreased expression of both DNAM-1 and TIGIT, although donor-specific changes did occur (Figure 2h). When assessing the underlying markers of $\bar{x}$EMD scores across all stIL15-γδ T cell donors, decreases in IdU, DNAM-1, TIGIT and increases in granzyme B underwent the most immunomodulation (Figure S4c). Collectively, these observations suggest that while stIL15-γδ T cells are potent PDO killers, cancer cells exert reciprocal effects on γδ T cell signalling and cell-state in a γδ T cell donor-dependent manner.

PDOs Reciprocally Immunomodulate γδ T Cell Phenotypes in a Patient-Specific Manner

To investigate whether the immunomodulation of γδ T cells by PDOs is a generalisable phenomenon of CRC-γδ T cell interactions, we performed an additional phenoscaping study of stIL15-γδ T cells from x4 proliferative and cytotoxic donors (A, B, E, and G) (Figure S5a) (Figure 1d-e) (Figure 2c-d) +/- x10 different CRC PDOs, +/- anti-B7-H3 mAb (Figure 3a). By using this systematic approach, we could directly compare the effects of inter-tumour heterogeneity (ITH), inter-donor heterogeneity (IDH), and multimodal γδ T cell killing in a single experimental design. Single-cell analysis of >5 million cells across x780 PDO-γδ T cell cultures revealed that γδ T cell signalling was determined not by γδ T cells IDH, but rather by ITH-specific interactions with PDOs (Figure 3b, Figure S5b).

Paired EMD scores were calculated between donor-matched stIL15-γδ T cells in monoculture or co-culture with CRC PDOs, with a positive or negative score indicating the up or downregulation of a marker by PDOs. Generally, PDOs negatively regulated γδ T cell PTM activatory signalling (pZAP70, pNF-κB, and pERK), effector function (granzyme B), and cell-state in a patient-specific manner (Figure 3c). Interestingly, γδ T cell pSTAT3 was up-regulated by multiple PDOs, consistent with previous reports of elevated STAT3 signalling and pSTAT3 communication between immune cells and CRC [50, 51]. PDOs also induced a global reduction in γδ T cell S-phase (Figure 3c) and checkpoint receptor expression (Figure 3d). The extent of stIL15-γδ modulation during AIC differed based on the PDO, with PDOs 11, 141 and 75 orchestrating the greatest change in γδ T cell phenotype (Figure 3e). γδ T cells were consistently altered by PDOs across all γδ T cell donors, with only minor evidence of IDH, highlighting the universal nature of immunomodulation by CRC cells (Figure 3f). This suggests that cancer cell ITH is dominant over γδ T cell IDH with regards to stIL15-γδ T cell signalling.

Crucially, despite the widespread downregulation of γδ T cell signalling by PDOs, the addition of anti-B7-H3 mAb rescued γδ T cell immunomodulation across all PDOs and PBMC donors (Figure 3e,f, Figure S5c-i). These results suggest that when stIL15-γδ T cells rely solely on AIC, their signalling and cell-state can be regulated by PDOs. However, when γδ T cells also engage ADCC, they can overcome cancer cell immunomodulation to restore their

cell-state and PTM signalling networks.

Reciprocal Inhibition of stIL15-γδ T Cell Signalling Limits Anti-CRC Cytotoxicity

The immune synapse between T cells and cancer cells involves multiple protein-protein interactions which govern downstream γδ T cell intracellular signalling cascades that determine anti-cancer cytotoxicity. We, therefore, sought to understand whether the immunomodulation of stIL15-γδ T cells by PDOs is associated with changes in anti-PDO cytotoxicity. In monoculture controls, PDOs were largely proliferative (pRB^{+}). However, when exposed to stIL15-γδ T cell AIC, PDO cells entered G0 (pRB^{-}) and apoptosis ($cPARP^{+}$). PDO apoptosis is further increased when stIL15-γδ T cells also perform ADCC via anti-B7-H3 mAb (Figure 4a) (Figure S6a).

By phenoscaping γδ T cells across multiple donors and patients, we could observe the respective impact of IDH and ITH on γδ T cell cytotoxicity. As expected, the susceptibility of PDOs to either AIC or ADCC varied across patients and γδ T cell donors (Figure 4b) (Figure S6b), with differences in ADCC not explained by PDO B7-H3 expression. Although most PDOs were susceptible to AIC, anti-B7-H3 mAb significantly improved cytotoxicity in 67.5% of PDOs (Figure 4b). Understanding which patients benefit from additional cytotoxicity in the presence of anti-B7-H3 mAb is therefore of importance.

ADCC is a dynamic process that is partially governed by target antigen positivity, target antigen density, effector FcγR expression, and antibody concentration. Work by ourselves and others has previously demonstrated that γδ T cell %CD16 expression and the degree of antigen expression strongly correlated with ADCC [8].

The susceptibility of PDOs to stIL15-γδ T cell killing did not correlate with stIL15-γδ T cell transduction efficiency, viability, or %γδ T cell purity at harvest from manufacture. This suggests that subtle variability in stIL15-γδ phenotypes between manufacturing batches did not account for the differences in killing observed (Figure S7a). All γδ T cell donors expressed CD16, but specific levels of %CD16 expression did not positively correlate with ADCC across the 10 CRC PDOs tested using 1 μg/mL of anti-B7-H3 mAb (Figure S7a) [8]. There were significant differences in antibody-mediated killing despite the 10 PDOs being 100% positive for extracellular B7-H3 expression (Figure S7b). Although B7-H3 antigen density varied across PDOs (Figure S7c), PDOs with higher B7-H3 antigen density were only susceptible to increased killing by γδ T cell donors E and G (Figure S7d). %CD16 expression by γδ T cells at the experiment endpoint also did not correlate with ADCC (Figure S7e). Despite being an activation marker with dynamic expression, the change in %CD16 following the addition of mAb (relative to co-culture controls) also did not correlate with anti-PDO cytotoxicity (Figure S7f). Together, these findings suggest that the susceptibility of 3D CRC PDOs to ADCC is not determined solely by B7-H3 antigen density and/or γδ T cell Fc receptor expression in the presence of 1 μg/mL mAb.

Due to their high tumour mutational burden (TMB), MSI CRC tumours typically respond well to immune checkpoint inhibition, whereas MSS CRC tumours with a low TMB typically do not [14]. Due to the MHC- and neoantigen-independent function of the γδ-TCR, Vγ9Vδ2 T cells have the potential to indiscriminately kill both MSI and MSS CRC tumours, rendering them attractive candidates for universal cytotoxicity against all CRC subsets. We found that stIL15-γδ T cells generally performed more AIC against MSI PDOs than MSS PDOs (Figure S7g-h). However, when stIL15-γδ T cells gained additional activation through B7-H3 opsonisation, this dichotomy disappeared, with stIL15-γδ T cells killing both MSI and MSS PDOs equally (Figure S7h). Furthermore, the addition of anti-B7H3 mAb increased cytotoxicity for both MSS and MSI PDOs (Figure S7h).

By phenoscaping γδ T cell PTM signalling and cancer cell death across x4 donors and x10 PDOs, we were able to observe broad trends in γδ T cell biology that are not specific to a single donor or PDO. Collectively, we found that across all donors and PDOs, anti-PDO AIC decreases when cancer cells suppress γδ T cell signalling (Figure 4c). This suggests that reciprocal immunomodulation of stIL15-γδ T cells limits anti-cancer cytotoxicity when γδ T cells use AIC alone. However, when stIL15-γδ T cells also engage ADCC against PDOs, stIL15-γδ T cell pro-inflammatory signalling is restored, and anti-cancer cytotoxicity is increased (Figure 4d). We found that while γδ T cells using AIC alone experienced global downregulation of PTM signalling, ADCC reactivated pZAP70, pSLP76, pNF-kB, pSTAT, pMAPK, and PI3K signalling flux and increased granzyme B expression across all PDOs and all γδ T cell donors (Figure 4e) (Figure S8a-b). These results suggest that the addition of exogenous opsonising anti-B7-H3 mAb to stIL15-γδ T cells can overcome cancer cell immunomodulation.

Anti-B7-H3 mAb Facilitates ADCC over Immune Checkpoint Blockade

B7-H3 can act as an immune checkpoint during innate and adaptive immune responses in certain contexts [52, 53]. To investigate whether B7-H3 mAb cytotoxicity occurs through ADCC and/or blockade of immune checkpoint inhibition, we co-cultured stIL15-γδ T cells with CRC PDOs with anti-B7-H3 IgG1 and an isogenic clone containing a mutated Fc domain that has a significantly reduced affinity for FcγRs on γδ T cells. TOB*iS* MC analysis revealed that PDO killing

was only achieved in the presence of B7-H3 mAb with functional Fc domains, with Fc-null mAb achieving no significant cytotoxicity over AIC controls (Figure 5a). Crucially, both IgG1 and Fc-null antibodies blocked the same B7-H3 epitope on CRC PDOs, indicating equal IgG paratope binding to PDO B7-H3 (Figure 5b). Furthermore, significant increases in stIL15-γδ T cell granzyme B expression were only observed in the presence of B7-H3 mAb with functional Fc domains (Figure 5c), correlating with anti-cancer ADCC (Figure 5a). Functional decreases in stIL15-γδ T cell DNAM-1 expression were also observed upon co-culture with PDO. There was a trend towards greater functional regulation of DNAM-1 expression in the presence of B7-H3 mAb with functional Fc domain (Figure 5d). Alongside B7-H3 CRISPR knockout data (Figure 2e), these data collectively demonstrate that B7-H3 mAb engages ADCC rather than immune checkpoint inhibition, resulting in reduced immunomodulation of stIL15-γδ T cells by CRC PDOs (Figure 4c-e).

CRC PDOs Re-wire stIL15-γδ T Cell Signalling Networks

To characterise how CRC PDO immunomodulation dysregulates stIL15-γδ T cell PTM signalling networks, we computed Density-Resampled Estimate of Mutual Information (DREMI) [33, 34] scores for all PTM-PTM pairs in stIL15-γδ T cell +/- CRC PDOs +/- B7-H3 mAb. The difference in DREMI score (ΔDREMI) for each PTM-PTM pair was calculated between stIL15-γδ T cell co-cultures and monoculture controls to assess immunomodulation of signalling networks by CRC PDOs.

ΔDREMI-PHATE analysis revealed that CRC PDOs re-wire γδ T cell PTM-PTM relationships in a patient-specific manner, with stIL15-γδ T cells from different donors converging on PDO-specific ΔDREMI profiles (Figure S9a,b). By contrast, the addition of B7-H3 mAb did not alter PTM-PTM relationships in any γδ T cell donors (Figure S9c-e). When combined with PTM signalling activity analysis (Figure 4c-e), these results suggest that CRC PDOs induce patient-specific rewiring of stIL15-γδ T cell PTM signalling networks during AIC immunomodulation, and this is unchanged by anti-B7-H3 ADCC. However, anti-B7-H3 ADCC provides an increased immunostimulatory signalling flux (within altered PTM networks) that permits increased γδ T cell effector function and degranulation (Figure S9).

Multimodal stIL15-γδ Cytotoxicity Kills Chemoresistant Revival Stem Cell PDOs

5-Fluorouracil (5-FU), Oxaliplatin, and Irinotecan are standard-of-care chemotherapies for CRC. All chemotherapies target mitotic processes and are therefore more effective in killing proliferative cancer cells compared to slow-cycling cancer cells. It has recently been shown that CRC tumours possess high levels of non-genetic plasticity [16] and that CRC cancer cells can rapidly switch between proliferative colonic stem cells (proCSCs) and slow-cycling revival colonic stem cells (revCSCs) [23]. Subsequent work has shown that proCSC are chemosensitive, whereas revCSC are chemorefractory [18]. Due to their chemoresistant nature, new therapeutic strategies to kill slow-cycling revCSC are urgently needed [12].

As γδ T cells do not target cancer cell proliferation we hypothesised that stIL15-γδ T cells could kill chemorefractory revCSC PDOs. To test this, we performed single-cell RNA sequencing (scRNA-seq) of the CRC PDOs used in this study and compared their relative proCSC to revCSC stem cell index [41] to chemotherapy and γδ T cell killing (Figure 6). This analysis revealed that CRC PDOs comprise an admixture of proCSC-like and revCSC-like cells, but PDOs dominated by revCSC cells are more chemoresistant (Figure 6a-d). However, we found that both stIL15-γδ T AIC (Figure 6e-f) and ADCC (Figure 6g-h) can kill CRC PDOs irrespective of stem cell admixture. γδ T cells that use combined AIC and ADCC multimodal cytotoxicity achieve the largest killing of both proCSC and revCSC CRC PDOs (Figure 6g-h). These results suggest that engineered γδ T cells are not susceptible to traditional chemorefractory mechanisms and can kill both chemosensitive proCSC and chemoresistant revCSC cancer cells.

Multimodal Killing Protects γδ T cells From Reciprocal Immunomodulation By Cancer Cells

Tumour resident γδ T cells receive a plethora of excitatory and inhibitory signalling cues that modulate their phenotype and anti-cancer cytotoxicity. Examples include TCR engagement; cytokine and chemokine exposure; Fc receptor engagement; immune checkpoint receptor-ligand engagement; extracellular matrix composition; the metabolic environment; and cell-cell interactions. In solid tumours, these cues are orchestrated by cancer cells to maintain an immunosuppressive TME. These cues are complex, combinatorial, and are transduced through intracellular T cell signalling networks to regulate anti-tumour immune responses. Therefore, as the master regulator of the TME, cancer cells regulate the anti-cancer cytotoxicity of biotherapeutics via the cues that govern their immunophenotype, PTM signalling, and cell-state.

To understand the overarching signalling dynamics of stIL15-γδ T cells +/- CRC PDOs +/- anti-B7-H3 mAb, we compiled data-driven signalling network models from >4 million stIL15-γδ T cells across x576 3D γδ T cell cultures (Figure 7). This analysis revealed that in monoculture, stIL15-γδ T cells benefit from constitutive JAK1/3 and STAT3/5 signalling as a result of stIL15 secretion which promotes granzyme B and perforin expression, and proliferation (Figure

7 (left)). When stIL15-γδ T cells kill PDOs using AIC alone, overwhelming inhibitory cues from cancer cells modulate and suppress γδ T cell signalling despite continued proliferation (Figure 7 (centre)). The specific type of γδ T cells immunomodulation is regulated by cancer cells, not PMBC donors, highlighting the importance of ITH in regulating T-cell signalling. However, when provided with additional immunoreceptor tyrosine-based activation motif (ITAM) signalling via an anti-B7-H3 mAb/Fc receptor axis, stIL15-γδ T cells can overcome cancer cell signalling repression, activate canonical γδ T cell PTM flux, and increase cancer cell killing over AIC alone (Figure 7 (right)). Collectively, these results suggest that cancer cell γδ T cell immunomodulation can be overcome using multimodal cytotoxicity.

Discussion

γδ T cells are gaining traction as an alternative chassis for the development of anti-cancer biotherapeutics. Their safety in the allogeneic setting, ease of engineering with pseudotyped lentiviral vectors, and variety of anti-cancer killing modalities provide a complementary alternative to traditional αβ-CAR T cells that rely on unimodal cytotoxicity against antigen-positive disease. Furthermore, γδ T cells have recently been described as immune effectors in MSI CRC with MHC class I defects following immune checkpoint blockade, able to compensate for the lack of conventional $CD8^+$ activity in this setting [54]. However, despite their initial promise, the treatment of solid tumours with unmodified γδ T cells has failed clinically — warranting the exploration of next-generation engineered γδ T cell biotherapeutics [55].

Owing to the enormous challenge posed by inter-tumour heterogeneity (ITH) in cancer, off-the-shelf biotherapeutics must be versatile when encountering patient-specific tumours. However, studying the interactions of biotherapeutics with heterogeneous cancer is further compounded by inter-donor heterogeneity (IDH), whereby donor-specific expansion, PTM signalling, and cytotoxicity profiles of cell therapies are determined by the healthy donor they were derived from. Adoptive cellular therapies are complex systems often relying on a plethora of cytotoxicity receptors, with γδ T cells able to kill cancer via multiple modalities including differential combinations of AIC and ADCC. Understanding the combinatorial interactions between ITH, IDH, and multimodal killing mechanisms is experimentally challenging. Here, through highly-multiplexed single-cell phenoscaping we were able to study the interplay between cancer ITH and Vγ9Vδ2 T cell IDH, AIC, and ADCC

TOB*iS* MC analysis revealed that unmodified γδ T cells struggle in 3D culture without exogenous cytokine or serum support, with significant apoptosis and poor proliferation after only 48 hours. However, γδ T cell viability could be rescued via ectopic expression of stIL15. Cytokine engineering of immune cells is becoming a common strategy, with IL-15-related technologies being assessed in αβ-CAR T cells [56], NK cells [57] and γδ T cells [58, 8]. Superagonism of JAK1/3 and STAT3/5 signalling is thought to promote proliferation, anti-cancer cytotoxicity, and persistence of biotherapeutics, as well as activation of receptive immune bystanders. Indeed, we show that stIL15 engineering improved γδ T cell manufacture, with increased proliferation (pRB^+, IdU^+), improved T cell activation (e.g. granzyme B^+, $perforin^+$, $CD69^+$), and decreased apoptosis ($cPARP^-$) compared to unmodified γδ T cells (Figure 1). Moreover, as a secreted product that can benefit receptive immune bystanders, we also found that stIL15 supported and maintained non-transduced γδ T cells *in vivo*, including $CD56^+$ NK cells (Figure S2). These results confirm that stIL15 γδ T cell engineering represents a promising route to overcome several of the limitations of unmodified γδ T cells.

Cancer cell recognition by γδ T cells involves a complex interplay of activatory and inhibitory receptors that is partially governed by the ligands expressed on cancer cells [5]. As γδ T cells from different donors also express varying levels of activatory and inhibitory receptors [59], generating universal anti-cancer γδ T cells from a range of donors is challenging without known biomarkers for donor selection. NK cell IDH has recently been shown to impact clinical outcomes, with biomarkers for donor selection requiring thorough investigation [60]. Moreover, unmodified γδ T cell IDH can contribute towards the varying cytotoxicity of γδ T cell products both *in vitro* and in human clinical trials [61, 62]. Our rationale for stIL15-engineering involves the generation of highly proliferative and universally cytotoxic γδ T cells from a range of donors that can survive in the immunosuppressive TME. Although stIL15 increased S-phase in all γδ T cell donors, we noticed a range of %S-phase responses that positively correlated with γδ T cell transduction efficiency (Figure 1d,e) (Figure S1f). This IDH-specific variance could be due to variable RDPro viral binding receptors across different γδ T cell donors, which are poorly understood in the context of the RDPro envelope.

PDOs are self-organising heterocellular systems that have gained popularity as a biomimetic 3D model system for the development of biotherapeutics against cancer [63, 64]. Unlike simple 2D monolayer cultures, PDOs require candidate biotherapeutics to kill cancer cells in a complex 3D ECM. As it is essential to consider ITH during pre-clinical development of anti-cancer therapeutics [19], we chose a panel of CRC PDOs spanning genetic (e.g., MSI/MSS and *KRAS*/*BRAF* /*APC* status), clinical stage, anatomical location, chemosensitivity, and colonic stem cell composition. Interestingly, despite the differences in γδ T cell IDH, the dominant factor governing γδ T cell PTM signalling, immunophenotype, and cytotoxicity was cancer cell ITH. These results suggest that cancer ITH is dominant over biotherapeutic IDH. We recently demonstrated that CRC PDO chemosensitivity aligns with cell-intrinsic cell-state

and PTM signalling, with slow-cycling PDOs (e.g., PDO 05, 11, 141 and 216) chemorefractory to standard-of-care drugs [18]. Here we show that chemorefractory PDOs have a higher revCSC-to-proCSC ratio. To our surprise, stIL15-γδ T cells can kill all CRC PDOs (Figure 4b) – including chemorefractory revCSC-dominant MSS CRC which represents patients with the greatest unmet clinical need (Figure 6) (Figure S7h). To our knowledge, this is the first demonstration that cellular therapies can kill chemorefractory revCSCs. Furthermore, despite orchestrating MHC-neoantigen-independent cytotoxicity, stIL15-γδ T cells also performed greater AIC against MSI PDOs (Figure S7h). Collectively, these results reinforce γδ T cells as a promising chassis for engineered adoptive cellular therapies against solid tumours, particularly if cytotoxicity can be performed against slow-cycling chemorefractory cell types.

Studies have investigated the expression of CD16 on γδ T cells against a variety of antigens expressed on both liquid and solid tumours [6, 7, 58, 8]. Recently, CD16 expression has gained attention as a biomarker of γδ T cell cytotoxicity even in the absence of mAb, whereby $CD16^{hi}$ donors performed substantially more AIC compared to $CD16^{lo}$ donors in models of ovarian cancer. However, γδ T cells engineered to express higher CD16 had no increase in their cytotoxicity, implying that the natural $CD16^{hi}$ or $CD16^{lo}$ status of γδ T cells is predictive of their cytotoxicity [58]. Using 1 µg/mL anti-B7-H3 mAb, we were unable to explain the differential susceptibility of CRC PDOs to ADCC based on the stIL15-γδ T %CD16 expression either post-manufacture or at the experiment endpoint (Figure S7a,e,f). Using a $B7\text{-}H3^{KO}$ PDO, we demonstrated that ADCC was B7-H3 antigen-specific and that the presence of B7-H3 in the parental PDO did not reduce the AIC performance of stIL15-γδ T cells (Figure 2e), despite reports that B7-H3 may inhibit the cytotoxicity of γδ T cells via downregulation of IFN-γ and granzyme B in CRC [65]. Furthermore, PDOs with higher B7-H3 antigen density were only susceptible to increased killing in the presence of B7-H3 mAb by two γδ T cell donors (Figure S7c,d). Encouragingly, we saw potent ADCC against CRC PDOs with relatively low B7-H3 density (<20,000 antigens/cell). Previous work assessing anti-B7-H3 CAR-T cells for the treatment of $B7\text{-}H3^{+}$ paediatric solid and liquid cancers demonstrated cytotoxicity against only medium and high B7-H3 antigen density models [66].

Within the immunosuppressive TME, adoptive cell therapies must navigate a complex interplay of both excitatory and inhibitory environmental signalling cues that govern their proliferation and cytotoxicity. Engineering strategies to 'armour' adoptive cell therapies to either augment their function or prevent TME inhibition include the secretion of cytokines, BiTEs and immune checkpoint inhibitors [67]. We provided γδ T cells with both stIL15 and exogenous mAb immunostimulatory agents to promote γδ T cell proliferation, anti-cancer cytotoxicity, and resistance to cancer cell suppression (Figure 7). We found that during AIC, stIL15-γδ T cells were vulnerable to a global reduction in S-phase (Figure 3c) that was not associated with cell-cycle exit or apoptosis (Figure S4a), demonstrating opposition to the mitogenic effect of stIL15 by CRC PDO immunomodulation. Surprisingly, CRC PDOs also exerted a reduction in stIL15-γδ T cell checkpoint receptor expression (Figure 3d), which may be due to reduced TCR activation [68] following the immunomodulation that contributed towards poor AIC. However, in the presence of anti-B7-H3 mAb these reductions in S-phase and checkpoint receptor expression were at least partially overcome (Figure S8) allowing increased cytotoxicity. For these reasons, future work combining B7-H3 mAb with immune checkpoint inhibitors would be particularly interesting. Recently stIL15-γδ T cells were also engineered to secrete an scFv-Fc against GD2 on *in vitro* and *in vivo* models of osteosarcoma, providing an ADCC self-autonomous biotherapeutic [8]. Furthermore, the self-secretion of opsonin also engaged ADCC-competent immune bystanders including NK cells, M1 macrophages, and neutrophils. Efficacy was observed against antigen-heterogeneous disease *in vivo* that was not controlled by a validated CAR-T cell model [8]. Aside from more traditional mAb and scFv-Fc proteins, a variety of immune cell engagers (ICE) are in development to encourage immune cell interaction with cancer, with specific engagers for γδ T cells, NK cells and myeloid cells being assessed [69]. Interestingly, approaches involving the FcγRs, CD16, and CD64; the natural cytotoxicity receptors (NCRs), NKp30 and NKp46; and NKD2D are undergoing pre-clinical evaluation, with many already entering clinical trials [69]. These alternative engagers have direct compatibility with stIL15-γδ T cells and could be used as additional armouring strategies to provide immunostimulatory signalling cues via tumour-associated antigens.

We demonstrate that opsonising CRC PDOs with B7-H3 mAb allows stIL15-γδ T cells to overcome cancer cell immunomodulation and perform potent cytotoxicity despite rewiring of PTM signalling networks by CRC PDOs. Therefore, engineering strategies that promote immunostimulation via the engagement of stabilised CD16 expression and more potent CD16 signalling may be of additional importance when designing ADCC-competent biotherapeutics, especially if they potentiate cytotoxicity in immunomodulating environments with rewiring of PTM signalling by cancer [70, 71]. Enzymatic cleavage of CD16 by the matrix metalloproteinase ADAM17 can be prevented by genetic modification of CD16 [72], which has been demonstrated in γδ T cells [58]. Furthermore, CD16 polymorphisms with increased affinity for mAb Fc binding (e.g., F158V polymorphism [73]) can be chosen during engineering of non-cleavable constructs [74], with a variety of non-cleavable, high-affinity CD16-engineered NK cells entering clinical trials [70]. Our central finding that using multiple killing mechanisms increases anti-cancer cytotoxicity and reduces γδ T cell suppression, supports future efforts to engage the polyfunctional nature of γδ T cells in adoptive cell therapies.

Despite the advent of multiple adoptive T cell therapies engineering approaches, translating promising *in vitro* and *in vivo* findings into the clinic remains a major challenge [75]. This complexity is further compounded by cancer ITH and T cell IDH. A detailed mechanistic understanding of how candidate cell therapies interact with biomimetic 3D models is emerging as an important pre-clinical step in biotherapeutic development. Through highly-multiplexed single-cell phenoscaping of hundreds of γδ T cell–cancer cell interactions – assessing PTM signalling, cell-state, apoptosis, and immunophenotype – we discovered that stIL15-γδ T cells that only kill by AIC can be immunomodulated by cancer cells in a ITH-dependant manner. However, stIL15-γδ T cells can overcome cancer cell immunomodulation by engaging ADCC to rapidly kill chemorefractory CRC cells. These results demonstrate the power of systematic pre-clinical phenoscaping of cellular therapies and reveal that multimodal γδ T cell killing can overcome cancer cell immunomodulation.

Declaration of Interests

J.A. declares founder shares in Autolus Ltd and collaborations with Roche and ALX-Oncology. M.B. is an inventor on patents pertaining to CAR-T cell development and the manufacture of γδ T cells (GB1821321.5, WO2023180759A1, WO2024009075A1). J.F. is an inventor on patents pertaining to engineered γδ T cells and methods for engineering γδ T cells which were used in this research (WO2021148788A1, WO2023180759A1). K.C. is an inventor on patent WO2021148788A1. DF is an inventor on patent WO2023180759A1.

Author Contributions

C.N. performed all γδ T cell-PDO experiments, analysed the data, and wrote the paper. R.O. performed all PDO SPLiT-seq experiments and analysis. D.F. performed γδ T cell analysis. C.H. and V.L. performed *in vivo* studies. P.V. performed γδ T cell-PDO experiments. J.S. developed TOB*iS* barcodes and conjugated rare-earth metal antibodies. E.B. conjugated rare-earth metal antibodies. M.R.Z. and F.C.R. provided computational analysis support. A.C. performed PDO CRISPR. A.K. manufactured and titred lentivirus. M.B. and K.C. provided anti-B7-H3 monoclonal antibody. J.A. Designed the study and analysed data. M.B. Designed the study and analysed data. J.F. conceived the project, designed the study, analysed the data, and wrote the paper. C.J.T. conceived the project, designed the study, analysed the data, and wrote the paper.

Acknowledgements

We are extremely grateful to M. Garnett, H. Francies and the Cell Model Network UK for sharing CRC PDOs. We thank Y. Guo and the UCL CI Flow-Core for CyTOF support, and both the GOSH-BRC and GOSH-ICH Flow Cytometry Core.

Funding and Manuscript Deposition

This work was supported by the UKRI Medical Research Council (MR/T028270/1), Cancer Research UK (C60693/A23783), Cancer Research UK City of London Centre (C7893/A26233), the UCLH Biomedical Research Centre (BRC422), the Cancer Research UK City of London Centre Clinical Academic Training Programme Award (C355/A28852), Cancer Research UK (CRUK) (CTRQQR-202100004), the Academy of Medical Sciences (SGL024/1022), the NIHR (CL-2019-18-007), the UCL Tech Fund (UTF-20-006/Fisher/UCL), the Little Princess Trust (CCLGA 2021 14 Fisher), the GOSH Charity (VS0119), and The Wellcome Trust (214046/Z/18/Z).

References

[1] J. J. Melenhorst et al. “Decade-long leukaemia remissions with persistence of CD4(+) CAR T cells”. In: *Nature* 602.7897 (2022), pp. 503–509.

[2] Bing Du et al. “CAR-T therapy in solid tumors”. In: *Cancer Cell* 43.4 (2025), pp. 665–679.

[3] J. Wagner et al. “CAR T Cell Therapy for Solid Tumors: Bright Future or Dark Reality?” In: *Mol Ther* 28.11 (2020), pp. 2320–2339.

[4] S. Mensurado, R. Blanco-Dominguez, and B. Silva-Santos. “The emerging roles of gammadelta T cells in cancer immunotherapy”. In: *Nat Rev Clin Oncol* 20.3 (2023), pp. 178–191.

[5] B. Silva-Santos, S. Mensurado, and S. B. Coffelt. “gammadelta T cells: pleiotropic immune effectors with therapeutic potential in cancer”. In: *Nat Rev Cancer* 19.7 (2019), pp. 392–404.

[6] J. P. Fisher et al. “Neuroblastoma killing properties of Vdelta2 and Vdelta2-negative gammadeltaT cells following expansion by artificial antigen-presenting cells”. In: *Clin Cancer Res* 20.22 (2014), pp. 5720–32.

[7] J. P. Fisher et al. “Effective combination treatment of GD2-expressing neuroblastoma and Ewing’s sarcoma using anti-GD2 ch14.18/CHO antibody with Vgamma9Vdelta2+ gammadeltaT cells”. In: *Oncoimmunology* 5.1 (2016), e1025194.

[8] D. Fowler et al. “Payload-delivering engineered gammadelta T cells display enhanced cytotoxicity, persistence, and efficacy in preclinical models of osteosarcoma”. In: *Sci Transl Med* 16.749 (2024), eadg9814.

[9] D. Fowler et al. “Payload Delivery: Engineering Immune Cells to Disrupt the Tumour Microenvironment”. In: *Cancers (Basel)* 13.23 (2021).

[10] Sattva Swarup Neelapu et al. “A phase 1 study of ADI-001: Anti-CD20 CAR-engineered allogeneic gamma delta (γδ) T cells in adults with B-cell malignancies”. In: *Journal of Clinical Oncology* 40.16$_{s}uppl$ (2022), pp. 7509–7509.

[11] Y. Xi and P. Xu. “Global colorectal cancer burden in 2020 and projections to 2040”. In: *Transl Oncol* 14.10 (2021), p. 101174.

[12] C. J. Tape. “Plastic persisters: revival stem cells in colorectal cancer”. In: *Trends Cancer* (2023).

[13] Y. Zhang et al. “Mechanisms of Immunosuppression in Colorectal Cancer”. In: *Cancers (Basel)* 12.12 (2020).

[14] M. Chalabi et al. “Neoadjuvant immunotherapy leads to pathological responses in MMR-proficient and MMR-deficient early-stage colon cancers”. In: *Nat Med* 26.4 (2020), pp. 566–576.

[15] K. Ganesh et al. “Immunotherapy in colorectal cancer: rationale, challenges and potential”. In: *Nat Rev Gastroenterol Hepatol* 16.6 (2019), pp. 361–375.

[16] J. Househam et al. “Phenotypic plasticity and genetic control in colorectal cancer evolution”. In: *Nature* (2022).

[17] S. B. Malla et al. “Pathway level subtyping identifies a slow-cycling biological phenotype associated with poor clinical outcomes in colorectal cancer”. In: *Nat Genet* 56.3 (2024), pp. 458–472.

[18] M. Ramos Zapatero et al. “Trellis tree-based analysis reveals stromal regulation of patient-derived organoid drug responses”. In: *Cell* 186.25 (2023), 5606–5619 e24.

[19] R. Fisher, L. Pusztai, and C. Swanton. “Cancer heterogeneity: implications for targeted therapeutics”. In: *Br J Cancer* 108.3 (2013), pp. 479–85.

[20] W. Yan et al. “The capability of heterogeneous gammadelta T cells in cancer treatment”. In: *Front Immunol* 14 (2023), p. 1285801.

[21] H. W. Song et al. “Manufacture of CD22 CAR T cells following positive versus negative selection results in distinct cytokine secretion profiles and gammadelta T cell output”. In: *Mol Ther Methods Clin Dev* 32.1 (2024), p. 101171.

[22] J. S. Fleck, J. G. Camp, and B. Treutlein. “What is a cell type?” In: *Science* 381.6659 (2023), pp. 733–734.

[23] X. Qin et al. “An oncogenic phenoscape of colonic stem cell polarization”. In: *Cell* 186.25 (2023), 5554–5568 e18.

[24] X. Qin et al. “Cell-type-specific signaling networks in heterocellular organoids”. In: *Nat Methods* 17.3 (2020), pp. 335–342.

[25] J. Sufi et al. “Multiplexed single-cell analysis of organoid signaling networks”. In: *Nat Protoc* 16.10 (2021), pp. 4897–4918.

[26] E. Mortier et al. “Soluble interleukin-15 receptor alpha (IL-15R alpha)-sushi as a selective and potent agonist of IL-15 action through IL-15R beta/gamma. Hyperagonist IL-15 x IL-15R alpha fusion proteins”. In: *J Biol Chem* 218.3 (2006), pp. 1612–1619.

[27] M. van de Wetering et al. “Prospective derivation of a living organoid biobank of colorectal cancer patients”. In: *Cell* 161.4 (2015), pp. 933–45.

[28] T. Sato et al. “Long-term expansion of epithelial organoids from human colon, adenoma, adenocarcinoma, and Barrett’s epithelium”. In: *Gastroenterology* 141.5 (2011), pp. 1762–72.

[29] Y. Takahashi et al. “A Refined Culture System for Human Induced Pluripotent Stem Cell-Derived Intestinal Epithelial Organoids”. In: *Stem Cell Reports* 10.1 (2018), pp. 314–328.

[30] K. Birley et al. “A novel anti-B7-H3 chimeric antigen receptor from a single-chain antibody library for immunotherapy of solid cancers”. In: *Mol Ther Oncolytics* 26 (2022), pp. 429–443.

[31] E. R. Zunder et al. “Palladium-based mass tag cell barcoding with a doublet-filtering scheme and single-cell deconvolution algorithm”. In: *Nat Protoc* 10.2 (2015), pp. 316–33.

[32] Soheil Kolouri, Gustavo K. Rohde, and Heiko Hoffmann. “Sliced Wasserstein Distance for Learning Gaussian Mixture Models”. In: (2018), pp. 3427–3436.

[33] S. Krishnaswamy et al. “Systems biology. Conditional density-based analysis of T cell signaling in single-cell data”. In: *Science* 346.6213 (2014), p. 1250689.

[34] D. van Dijk et al. “Recovering Gene Interactions from Single-Cell Data Using Data Diffusion”. In: *Cell* 174.3 (2018), 716–729 e27.

[35] K. R. Moon et al. “Visualizing structure and transitions in high-dimensional biological data”. In: *Nat Biotechnol* 37.12 (2019), pp. 1482–1492.

[36] A. B. Rosenberg et al. “Single-cell profiling of the developing mouse brain and spinal cord with split-pool barcoding”. In: *Science* 360.6385 (2018), pp. 176–182.

[37] S. Parekh et al. “zUMIs - A fast and flexible pipeline to process RNA sequencing data with UMIs”. In: *GigaScience* 7.6 (May 2018), giy059.

[38] F. A. Wolf, P. Angerer, and F. J. Theis. “SCANPY: large-scale single-cell gene expression data analysis”. In: *Genome Biol* 19.1 (2018), p. 15.

[39] S. L. Wolock, R. Lopez, and A. M. Klein. “Scrublet: Computational Identification of Cell Doublets in Single-Cell Transcriptomic Data”. In: *Cell Syst* 8.4 (2019), 281–291 e9.

[40] R. Satija et al. “Spatial reconstruction of single-cell gene expression data”. In: *Nat Biotechnol* 33.5 (2015), pp. 495–502.

[41] Ester Gil Vasquez et al. “Dynamic and Adaptive Cancer Stem Cell Population Admixture in Colorectal Neoplasia”. In: *Cell Stem Cell* 29 (2022), pp. 1213–1228.

[42] K. E. de Visser and J. A. Joyce. “The evolving tumor microenvironment: From cancer initiation to metastatic outgrowth”. In: *Cancer Cell* 41.3 (2023), pp. 374–403.

[43] X. Chen et al. “The effects of metabolism on the immune microenvironment in colorectal cancer”. In: *Cell Death Discov* 10.1 (2024), p. 118.

[44] X. Zhou et al. “I-TASSER-MTD: a deep-learning-based platform for multi-domain protein structure and function prediction”. In: *Nat Protoc* 17.10 (2022), pp. 2326–2353.

[45] DY. Orlova et al. “Earth Mover’s Distance (EMD): A True Metric for Comparing Biomarker Expression Levels in Cell Populations”. In: *PLOS ONE* 11.3 (Mar. 2016), pp. 1–14.

[46] J. Fisher et al. “Engineering γδT cells limits tonic signaling associated with chimeric antigen receptors”. In: *Science Signaling* 12.598 (2019), eaax1872.

[47] S. Modak et al. “Monoclonal antibody 8H9 targets a novel cell surface antigen expressed by a wide spectrum of human solid tumors”. In: *Cancer Res* 61.10 (2001), pp. 4048–54.

[48] C. Wang et al. “Potential Therapeutic Targets of B7 Family in Colorectal Cancer”. In: *Front Immunol* 11 (2020), p. 681.

[49] K. Feustel, J. Martin, and G. S. Falchook. “B7-H3 Inhibitors in Oncology Clinical Trials: A Review”. In: *J Immunother Precis Oncol* 7.1 (2024), pp. 53–66.

[50] Y. Fan, R. Mao, and J. Yang. “NF-kappaB and STAT3 signaling pathways collaboratively link inflammation to cancer”. In: *Protein Cell* 4.3 (2013), pp. 176–85.

[51] A. N. Gargalionis, K. A. Papavassiliou, and A. G. Papavassiliou. “Targeting STAT3 Signaling Pathway in Colorectal Cancer”. In: *Biomedicines* 9.8 (2021).

[52] J. Leitner et al. “B7-H3 is a potent inhibitor of human T-cell activation: No evidence for B7-H3 and TREML2 interaction”. In: *Eur J Immunol* 39.7 (2009), pp. 1754–64.

[53] C. Chen et al. “Induced expression of B7-H3 on the lung cancer cells and macrophages suppresses T-cell mediating anti-tumor immune response”. In: *Exp Cell Res* 319.1 (2013), pp. 96–102.

[54] N. L. de Vries et al. “gammadelta T cells are effectors of immunotherapy in cancers with HLA class I defects”. In: *Nature* 613.7945 (2023), pp. 743–750.

[55] C. Q. Wang, P. Y. Lim, and A. H. Tan. “Gamma/delta T cells as cellular vehicles for anti-tumor immunity”. In: *Front Immunol* 14 (2023), p. 1282758.

[56] Y. Chen et al. “Eradication of Neuroblastoma by T Cells Redirected with an Optimized GD2-Specific Chimeric Antigen Receptor and Interleukin-15”. In: *Clin Cancer Res* 25.9 (2019), pp. 2915–2924.

[57] R. N. Silvestre et al. “Engineering NK-CAR.19 cells with the IL-15/IL-15Ralpha complex improved proliferation and anti-tumor effect in vivo”. In: *Front Immunol* 14 (2023), p. 1226518.

[58] D. Lee et al. “Unlocking the potential of allogeneic Vdelta2 T cells for ovarian cancer therapy through CD16 biomarker selection and CAR/IL-15 engineering”. In: *Nat Commun* 14.1 (2023), p. 6942.
[59] L. A. Ridgley et al. “Releasing the restraints of Vgamma9Vdelta2 T-cells in cancer immunotherapy”. In: *Front Immunol* 13 (2022), p. 1065495.
[60] T. J. Laskowski, A. Biederstadt, and K. Rezvani. “Natural killer cells in antitumour adoptive cell immunotherapy”. In: *Nat Rev Cancer* 22.10 (2022), pp. 557–575.
[61] P. L. Ryan et al. “Heterogeneous yet stable Vdelta2(+) T-cell profiles define distinct cytotoxic effector potentials in healthy human individuals”. In: *Proc Natl Acad Sci U S A* 113.50 (2016), pp. 14378–14383.
[62] R. E. Burnham et al. “Characterization of Donor Variability for gammadelta T Cell ex vivo Expansion and Development of an Allogeneic gammadelta T Cell Immunotherapy”. In: *Front Med (Lausanne)* 7 (2020), p. 588453.
[63] F. Jacob, G. L. Ming, and H. Song. “Generation and biobanking of patient-derived glioblastoma organoids and their application in CAR T cell testing”. In: *Nat Protoc* 15.12 (2020), pp. 4000–4033.
[64] J. F. Dekkers et al. “Uncovering the mode of action of engineered T cells in patient cancer organoids”. In: *Nat Biotechnol* 41.1 (2023), pp. 60–69.
[65] H. Lu et al. “B7-H3 inhibits the IFN-gamma-dependent cytotoxicity of Vgamma9Vdelta2 T cells against colon cancer cells”. In: *Oncoimmunology* 9.1 (2020), p. 1748991.
[66] R. G. Majzner et al. “CAR T Cells Targeting B7-H3, a Pan-Cancer Antigen, Demonstrate Potent Preclinical Activity Against Pediatric Solid Tumors and Brain Tumors”. In: *Clin Cancer Res* 25.8 (2019), pp. 2560–2574.
[67] E. R. Hawkins, R. R. D’Souza, and A. Klampatsa. “Armored CAR T-Cells: The Next Chapter in T-Cell Cancer Immunotherapy”. In: *Biologics* 15 (2021), pp. 95–105.
[68] Z. Gao et al. “Gamma delta T-cell-based immune checkpoint therapy: attractive candidate for antitumor treatment”. In: *Mol Cancer* 22.1 (2023), p. 31.
[69] A. Fenis et al. “New immune cell engagers for cancer immunotherapy”. In: *Nat Rev Immunol* (2024).
[70] C. Capuano et al. “Harnessing CD16-Mediated NK Cell Functions to Enhance Therapeutic Efficacy of Tumor-Targeting mAbs”. In: *Cancers (Basel)* 13.10 (2021).
[71] K. J. Dixon, J. Wu, and B. Walcheck. “Engineering Anti-Tumor Monoclonal Antibodies and Fc Receptors to Enhance ADCC by Human NK Cells”. In: *Cancers (Basel)* 13.2 (2021).
[72] R. Romee et al. “NK cell CD16 surface expression and function is regulated by a disintegrin and metalloprotease-17 (ADAM17)”. In: *Blood* 121.18 (2013), pp. 3599–608.
[73] H. R. Koene et al. “Fc gammaRIIIa-158V/F polymorphism influences the binding of IgG by natural killer cell Fc gammaRIIIa, independently of the Fc gammaRIIIa-48L/R/H phenotype”. In: *Blood* 90.3 (1997), pp. 1109–14.
[74] H. Zhu et al. “Pluripotent stem cell-derived NK cells with high-affinity noncleavable CD16a mediate improved antitumor activity”. In: *Blood* 135.6 (2020), pp. 399–410.
[75] A. Daei Sorkhabi et al. “The current landscape of CAR T-cell therapy for solid tumors: Mechanisms, research progress, challenges, and counterstrategies”. In: *Front Immunol* 14 (2023), p. 1113882.

Figure Legends

Figure 1. Secreted stIL15 Supports γδ T Cells Without Exogenous Cytokines in 3D. a) Experimental design. γδ T cells were expanded from x7 healthy donors, either unmodified or transduced to overexpress stIL15, cultured in 3D without IL-2 or FBS, and analysed by thiol-reactive organoid barcoding *in situ* mass cytometry (TOB*iS* MC). **b)** Flow cytometry immunophenotyping of unmodified and stIL15-γδ T cells after 12-day expansion (n=38-80 across 7 donors). Comparison by paired *t* -test. **c)** Following TOB*iS* MC, $CD45^{+}CD3^{+}$γδ-TCR^{+} events were gated and exported for analysis. PCA of x42 3D cultures with single-cell PHATE density embeddings from unmodified and stIL15 transduced γδ T cell raw expression data. **d)** γδ T cell cell-states. Mean +/- SD of triplicate samples. **e)** γδ T cell % S-phase. Comparisons by 2-way ANOVA with Tukey's multiple comparisons test. **f)** EMD heatmap of γδ T cell PTM signalling and immunophenotyping markers. EMD scores were calculated between unmodified and stIL15-γδ T cells for each donor. **, $p < 0.01$; ***, $p < 0.001$; ****, $p < 0.0001$. n.s., not significant.

Figure 2. Single-Cell Phenoscaping of γδ T cell Anti-PDO Cytotoxicity. a) Experimental design and PDO27 B7-H3 expression measured by flow cytometry. **b)** γδ T cell EMD PHATE at phenoscape (middle) and single-cell (inserts) resolution. x180 γδ T cell–PDO cultures. EMD scores were calculated relative to unmodified-γδ monoculture controls to capture changes during stIL15 transduction and γδ co-culture with PDO **c)** γδ T PHATE annotated by PDO apoptosis. **d)** therapeutic apoptosis via AIC or ADCC per γδ T cell donor. Mean +/- SD of triplicate samples. 2-way ANOVA with Sidak's multiple comparisons test. Grey bar compares AIC; orange bar compares cytotoxicity from AIC + B7-H3 mAb. **e)** ADCC killing in parental and B7-H3 CRISPR knockout PDO 27 demonstrate antigen specificity of ADCC killing. Unpaired *t* -test (apoptosis values). Mean +/- SD of quintuplet samples. **f)** $\bar{x}$EMD of γδ T cells in monoculture or co-culture with PDO27. Mean of six replicate samples per donor. The reference for $\bar{x}$EMD scores for all conditions, including monoculture conditions, were calculated relative to monoculture controls. **g)** γδ T cell S-phase +/- PDOs. 6 replicates per donor, overall mean across all donors plotted. 2-way ANOVA with Tukey's multiple comparisons test. **h)** EMD heatmap of stIL15-γδ T cell PTM signalling and immunophenotyping markers +/- B7-H3 mAb compared to monoculture controls for each stIL15-γδ T cell donor. EMD scores were calculated relative to monoculture controls for each donor and treatment. **, $p < 0.01$; ***, $p < 0.001$; ****, $p < 0.0001$. n.s., not significant.

Figure 3. PDOs Reciprocally Regulate γδ T cell Phenotypes in a Patient-Specific Manner. a) Experimental overview. **b)** stIL15-γδ EMD-PHATE phenoscape annotated by PDO. EMD scores were calculated relative to stIL15-γδ monoculture controls to capture changes during γδ co-culture with PDO. **c)** γδ T cell PTM and immunophenotype response to PDOs, including changes in S-phase (IdU). **d)** Percentage change in immunophenotype marker expression in response to PDOs relative to monoculture controls. **e)** $\bar{x}$EMD of γδ T cells killing PDOs either by AIC or in the presence of B7-H3 mAb, coloured by PDO, or **f)** γδ T cell donor. One-way ANOVA with Tukey's multiple comparisons test. *, $p < 0.05$; **, $p < 0.01$; n.s., not significant.

Figure 4. Regulation of γδ T cells Correlates with anti-PDO Cytotoxicity. a) Single-cell PHATE of x10 PDOs + stIL15-γδ T cells +/- B7-H3 mAb. **b)** PDO apoptosis via AIC or ADCC per γδ T donor across x10 PDOs. 2-way ANOVA with Sidak's multiple comparisons test. Mean +/- SD of triplicate samples. **c)** Correlation of γδ $\bar{x}$EMD with anti-PDO cytotoxicity during AIC, coloured by γδ granzyme B. τ denotes the Kendall rank correlation coefficient. **d)** Correlation of γδ $\bar{x}$EMD with anti-PDO cytotoxicity + B7-H3 mAb, coloured by γδ granzyme B. τ denotes the Kendall rank correlation coefficient. **e)** stIL15-γδ PTM signalling with PDOs +/- B7-H3 mAb. *, $p < 0.05$; **, $p < 0.01$; ***, $p < 0.001$; ****, $p < 0.0001$.

Figure 5. B7-H3 mAb Facilitates Fc-receptor-dependant ADCC by stIL15-γδ T cells. a) Therapeutic apoptosis by stIL15-γδ T cells +/- mAb +/- mAb (Fc null), against CRC PDO 141. 2-way ANOVA with Dunnett's multiple comparisons test. Mean +/- SD of triplicate samples. **b)** Correlation between therapeutic apoptosis and B7-H3 epitope availability. The same clone of B7-H3 mAb was conjugated into the CyTOF staining panel to calculate the relative availability of B7-H3 epitope. **c)** EMD scores of stIL15-γδ T cell granzyme B expression calculated relative to untreated co-culture controls. One-way ANOVA with Sidak's multiple comparisons test. Mean +/- SD of triplicate samples. **d)** Decrease in stIL15-γδ T cell % DNAM-1 expression relative to monoculture controls for each treatment. One-way ANOVA with Sidak's multiple comparisons test. Mean +/- SD of triplicate samples. *, $p < 0.05$; ***, $p < 0.001$; ****, $p < 0.0001$; n.s., not significant.

Figure 6. γδ T Cells Can Kill Chemorefractory revCSC CRC PDOs. a-b) Chemotherapy-induced apoptosis per PDO across a range of chemotherapy concentrations (SN-38 (1 nM - 100 nM), 5-FU (0.2 μM - 200 μM), and oxaliplatin (2 nM - 200 nM))[18]. **c-d)** scRNA-seq stem cell index scores (Z-score) of CRC PDOs ranked from proCSC- to revCSC-enriched. 1 dot = 1 cell. Box and whisker = median + quartiles. Unpaired *t* -test between mean PDO stem cell indexes. e-f) Therapeutic apoptosis by stIL15-γδ T cells alone, or **g-h)** with B7-H3 mAb. Mean +/- SD. Comparisons by unpaired *t*-test. ****, $p < 0.0001$. n.s., not significant.

Figure 7. Multimodal γδ T Cell Cytotoxicity Overcomes Cellular Therapy Immunomodulation. γδ T cell signalling networks following stIL15 transduction, co-culture with PDO and addition of B7-H3 mAb. Nodes are coloured by γδ EMD scores computed

from >4 million cells across 576 conditions. (Bottom) γδ cell-state histograms. Each cell-state phase is presented as mean +/- SD (n=129-138).

Figure 1

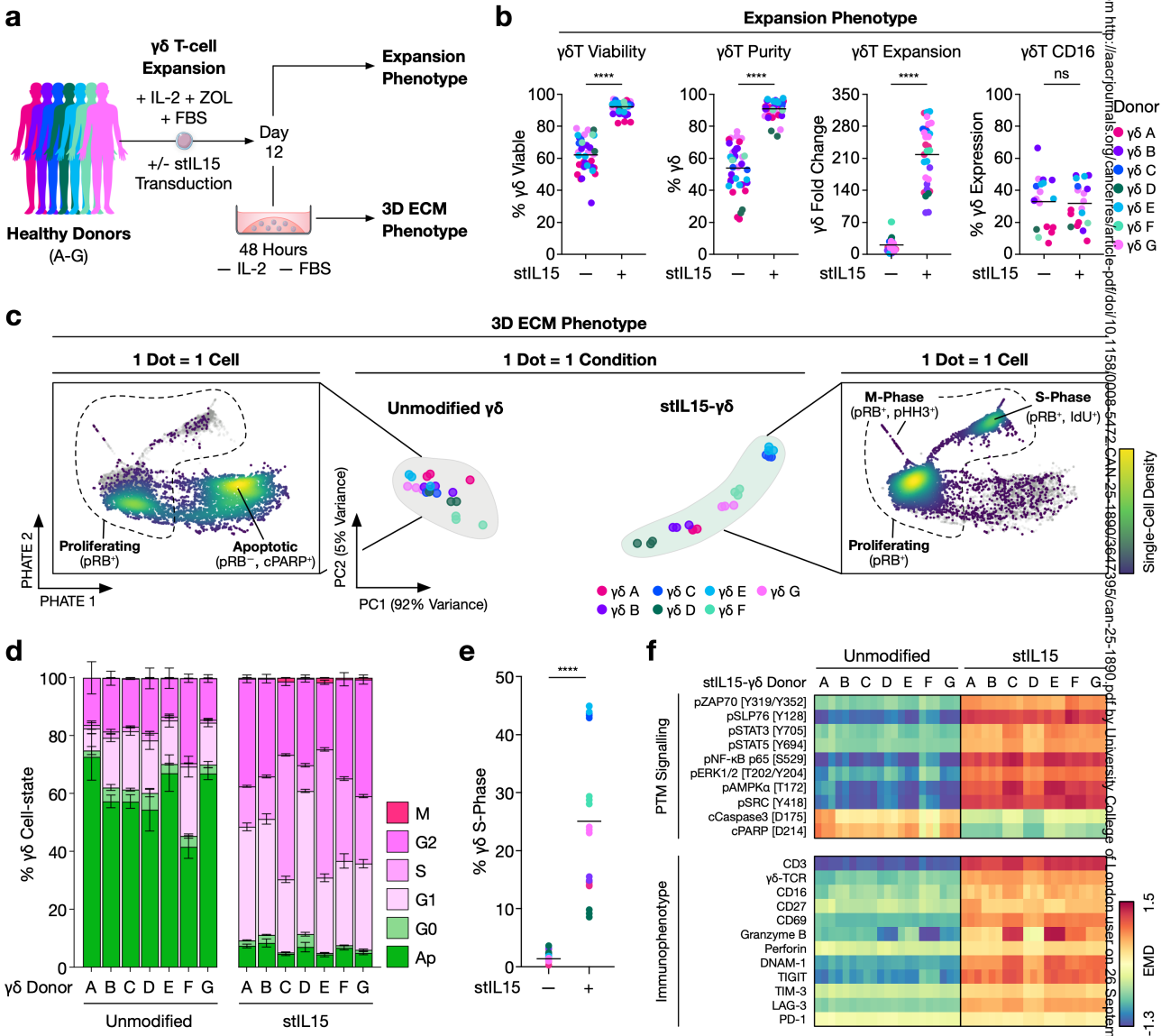

Figure 2

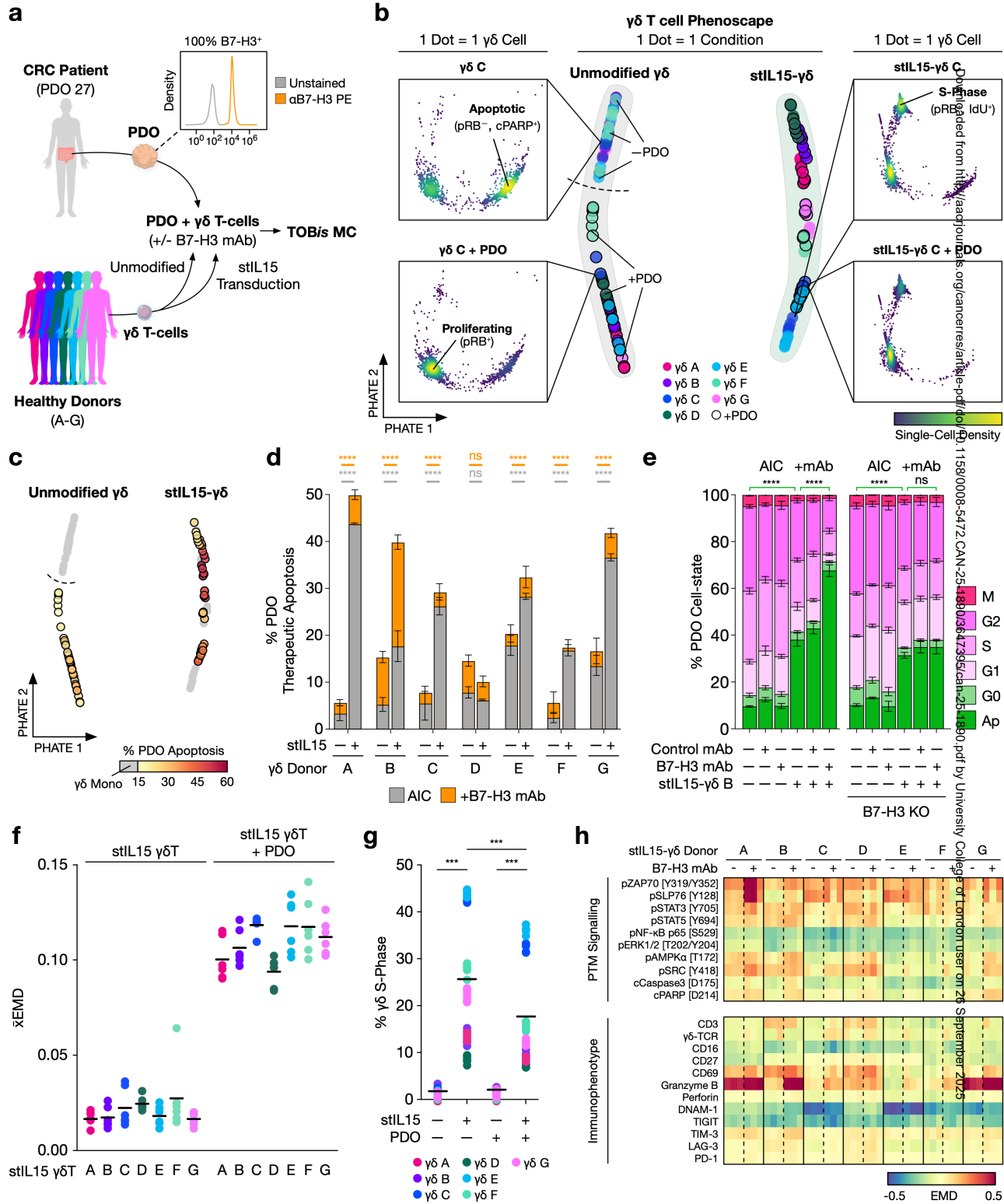

Figure 3

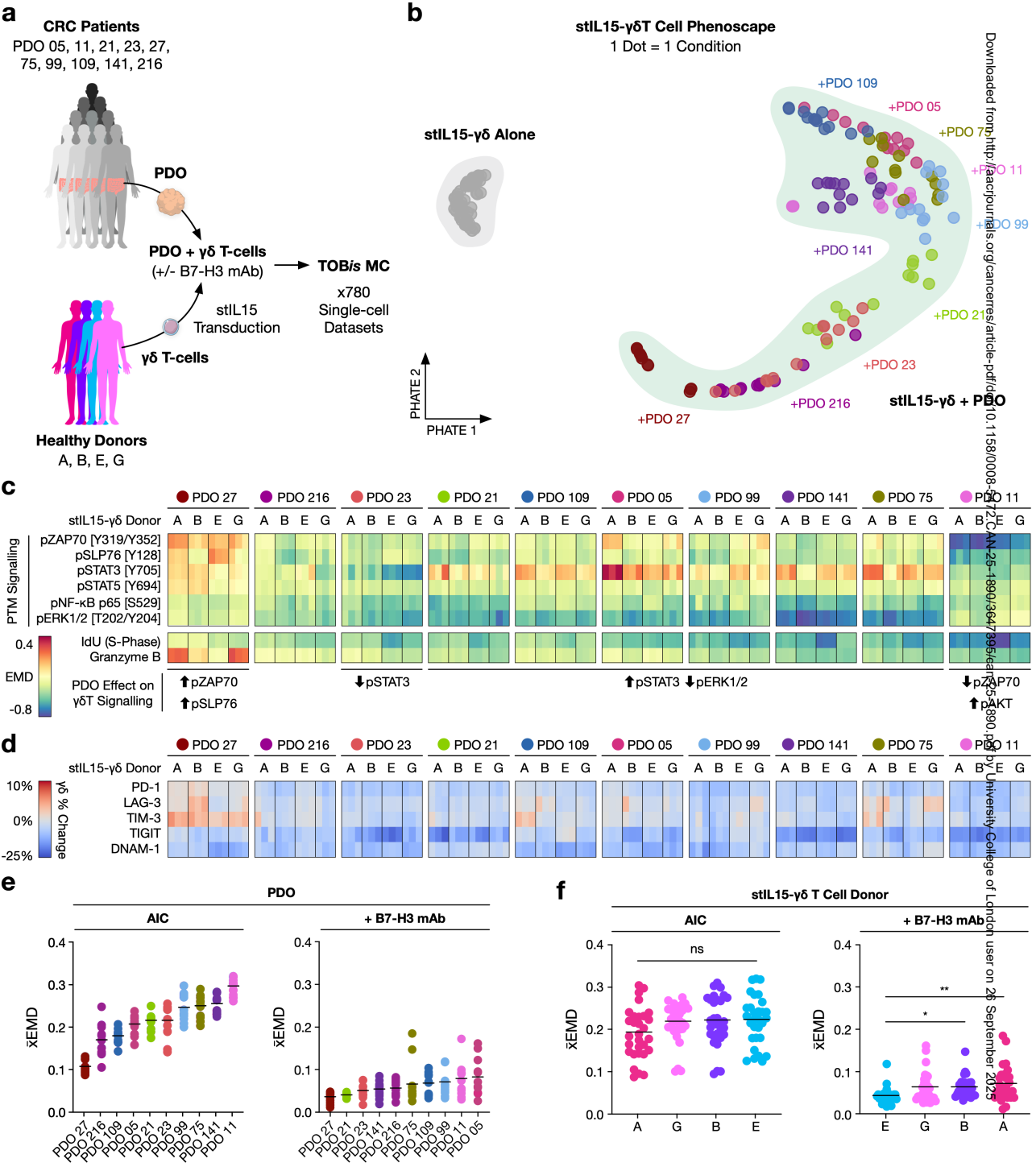

Figure 4

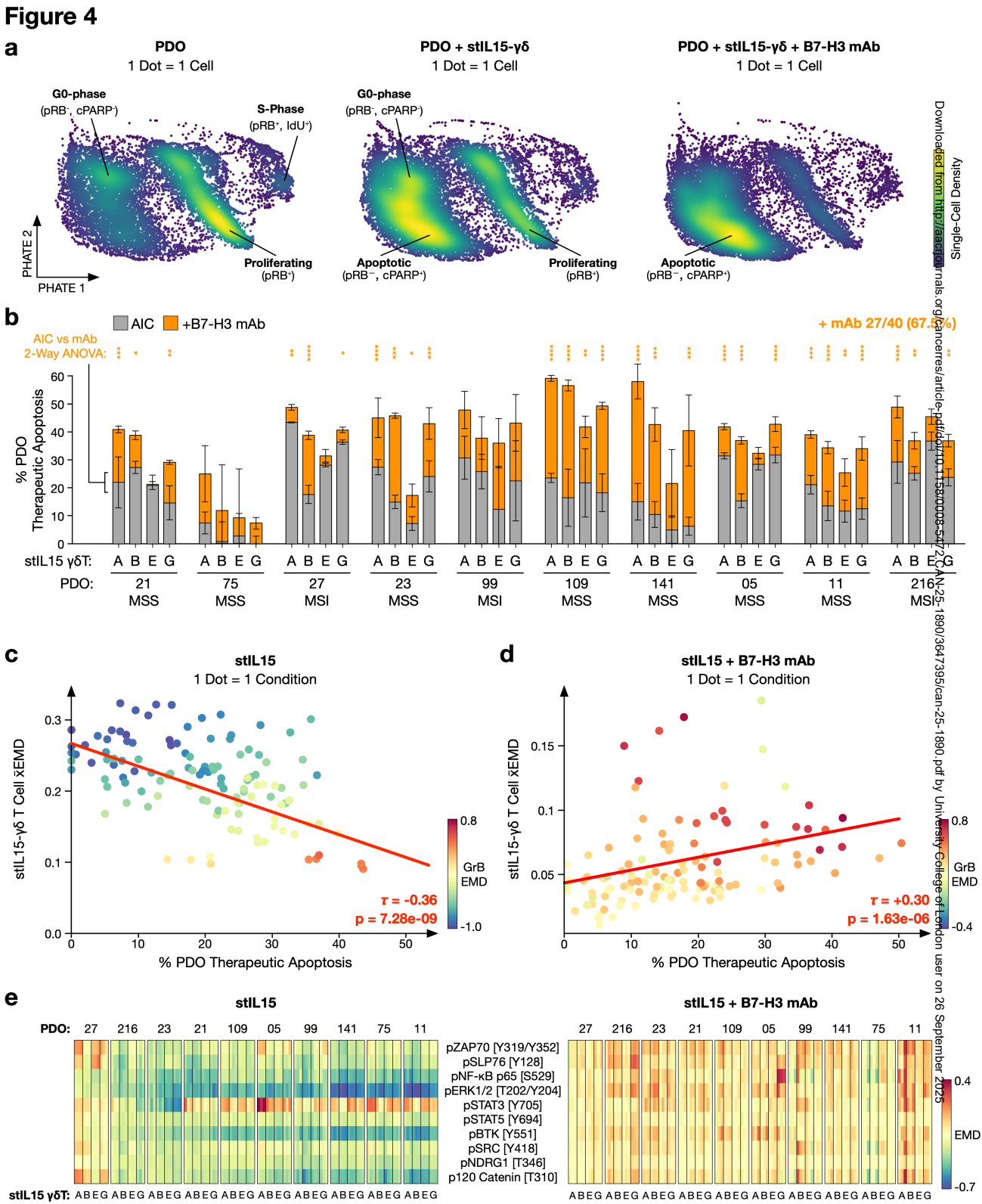

Figure 5

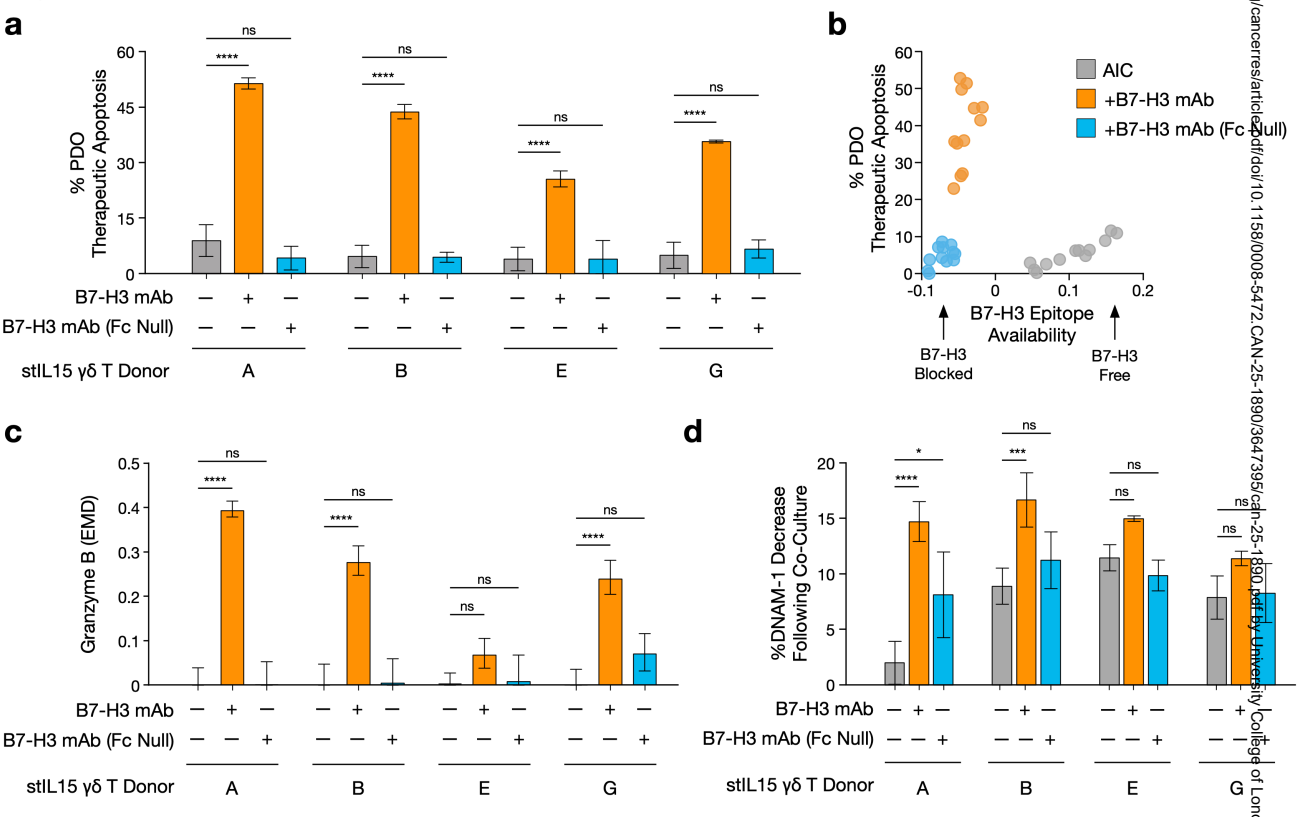

Figure 6

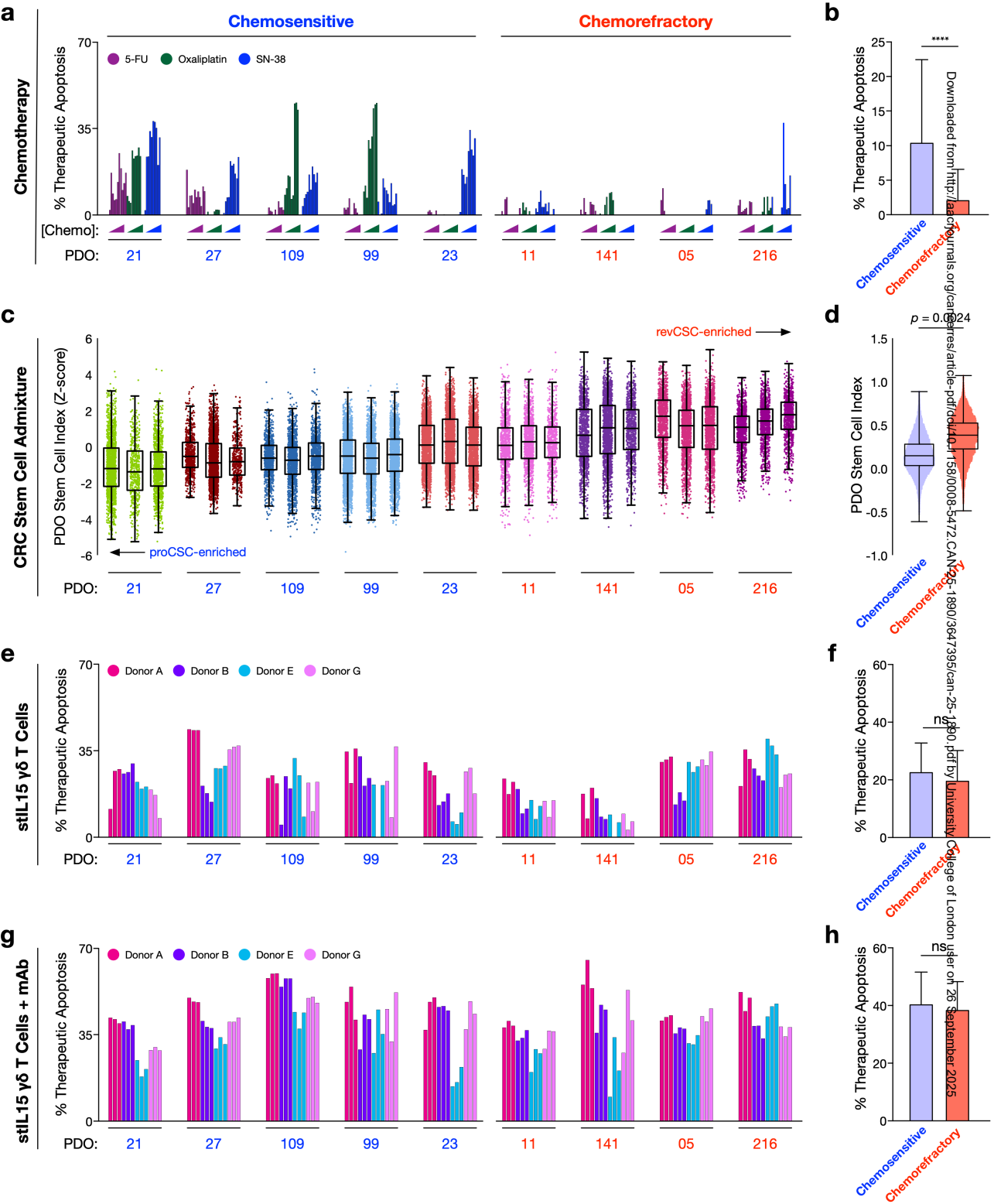

Figure 7